The role of low-level winds on the morning transition in Dallas-Fort Worth

By

Kip F. Nielsen

Submitted to the graduate degree program in the Department of Geography & Atmospheric Science and the Graduate Faculty of the University of Kansas in partial fulfillment of the requirements for the degree of Master of Science.

Chair: Dr. David A. Rahn

Dr. David B. Mechem

Dr. Nathaniel A. Brunsell

Date Defended: 18 May 2021

The thesis committee for Kip F. Nielsen certifies that this is the approved version of the following thesis:

The role of low-level winds on the morning transition in Dallas-Fort Worth

Chair: Dr. David A. Rahn

Date Approved: 18 May 2021

Abstract

In highly urbanized areas, anthropogenic changes to the landscape lead to the well-known urban heat island (UHI) where the temperature over urban areas is warmer than the surrounding rural regions. This urbanization modifies the temperature profile above the city and its connection to the mixed-layer depth is related to health risks including heat stress and respiratory illness that are linked with air pollution. This work focuses on the morning transition, which is defined as starting at dawn and ending at the onset of the rapid growth of the mixed layer. Mean temperature and wind profiles are compiled every half-hour from aircraft landing and departing Dallas-Fort Worth International (DFW) and Dallas Love Field (DAL) from 2010 to 2019 using data provided by the Aircraft Meteorological Data Relay (AMDAR) program. The Dallas-Fort Worth area is selected as the study region due to its large urban area that is located in the central Great Plains with no major topographic features or coastal influences. Results using a Richardson number formulation with a threshold of 0.25 offers the best characterization of boundary layer (BL) height. Observations with cloud oktas less than five are selected to eliminate transient weather events and top-down forcings caused by cloudy conditions that impact the BL more than local effects. Strong northerly winds can be associated with clear, post-frontal conditions, so southerly winds are selected. The results show greater BL heights at dawn in the summer than in the winter. A breakpoint algorithm using piecewise linear regression on the diurnal BL height from four hours before dawn to ten hours after dawn offers the most reasonable approach to determine the end of the morning transition. Changing the start and end of the hours used in the breakpoint calculation or the Richardson number threshold from 0.20 to 0.30 does not significantly affect the morning transition durations. In the summer, stronger winds are associated with a more well-mixed layer at dawn when the morning transition starts. Stronger

low-level winds at dawn lead to a weaker nocturnal temperature inversion and a shorter morning transition once insolation generates thermally-driven turbulence. This suggests that the Great Plains low-level jet is the primary factor for shorter morning transitions, earlier rapid mixed layer growth, and a quicker mixing of pollutants from the morning commute using a much larger dataset than previous studies.

Acknowledgments

I would first like to thank my advisor, Dr. David Rahn, for his patience, kindness, and helpful support throughout this project. His help was invaluable and there's no way I would have been able to do this project without him. I would also like to thank my other two committee members, Dr. David Mechem and Dr. Nathaniel Brunsell, for their prompt and welcoming assistance. If I ever needed help with anything they were always just a quick email away. I also thank the faculty and staff of the Department of Geography and Atmospheric Science. All the courses I took aided in this project one way or another, whether that was learning how to use Arc GIS or a general improvement of my programming skills in Python.

I am filled with gratitude for the friendships made along the way and all the support from my family. It's great to see so many strong friendships last throughout the ultimate test of a global pandemic. This includes everything from pre-pandemic trivia nights to Zoom study sessions. It will be fun to see everyone's path going forward. Last, and certainly not least, I would like to thank my family for the loving support. When everything went online, they were right there to still make it a fun experience. Their constant curiosity about my project taught me new ways of explaining it to people with different backgrounds. I am eternally grateful to have had such a wonderful experience over the past couple years and I'm excited for what's to come!

Table of Contents

List of Figures

List of Tables

1. Introduction

a. Motivation and Research objectives

Anthropogenic impacts on landscapes are easily seen in highly urbanized areas and lead to the well-known urban heat island (UHI) where the temperature over urban areas is warmer than the surrounding rural regions (Oke 1987). The impacts of urbanization on atmospheric processes can be challenging to quantify, but getting a more thorough understanding of urban areas is important since the world's population is anticipated to reach 10 billion by 2100 and 90% of that population is expected to reside in urban areas (United Nations 2011). Along with an increase in population comes an increase in energy usage that contributes to more pollution and waste heat that amplifies the UHI. It is estimated that approximately 60-80% of the global energy use is consumed by urban areas (Global Energy Assessment Writing Team 2012). Urban areas are increasing worldwide, four states in the United States are expected to be at least half covered with urban land by 2050 and urban land in the United States is projected to double between 2010 and 2060 (Seto et al. 2011; Nowak and Walton 2005; Nowak and Greenfield 2018). With this comes various health risks such as contaminated drinking water, inadequate solid and industrial waste, and the everlasting connection with poverty and unemployment. Furthermore, an increase in ozone, smog, and other harmful pollutants can expose millions to unsafe air quality levels. Past studies (Li et al. 2017; Barlow 2014; Grimmond 2006) investigated the lowest part of the atmosphere over cities, but cite that progress is inhibited by an insufficient temporal, vertical, and spatial resolution of observations. By using temperature and wind speed profiles to diagnose the vertical structure and processes in the lower part of the atmosphere over an urban area, important characteristics can be quantified. This includes the stability of the lower atmosphere,

which is connected to the UHI and related to the concentration of pollution near the surface that impacts the cardiovascular and respiratory health of individuals. Given the importance of temperature and wind speed profiles over cities and the lack of observations that have inhibited progress, this project pursues three broad objectives:

1. Assess the ability of atmospheric observations from commercial aircraft to depict the evolution of the lower atmosphere at half-hourly intervals.
2. Determine the base climatological features.
3. Investigate the role of low-level winds in explaining the day-to-day variability of the lower atmosphere.

This work focuses on the Dallas-Fort Worth area due to its large urban extent that is in the central Great Plains with no major topographic features or coastal influences. There are also ample surface observing meteorological stations and observations from commercial aircraft departing and arriving at airports in Dallas-Fort Worth through the Aircraft Meteorological Data Relay (AMDAR) program that provide sufficient profiles of the atmosphere.

b. Background

i. Boundary layer

The planetary boundary layer (BL) is the lowest part of the atmosphere that is directly influenced by the surface and is impacted by a wide variety of forcing mechanisms and meteorological controls. Its diurnal evolution is heavily dependent on incoming solar radiation, outgoing longwave radiation, sensible heat (SH), and latent heat (LH). At sunrise, incoming solar radiation causes a preexisting nocturnal stable layer to slowly become eroded until thermals from

the surface reach the height of the residual layer. Convection then rapidly increases the height of the BL and forms a deep mixed layer. Buoyant air parcels that overshoot the level of neutral buoyancy reach a layer called the entrainment zone. Clouds begin to form at the lifting condensation level and can become a problem when using lidar backscatter measurements to detect the top of the mixed layer (Hennemuth and Lammert 2006). Thermal convection is suppressed when the sun goes down, although some shallow nocturnal convection can continue to exist over urban areas. A residual layer forms from the remnants of the daytime deep mixed layer. The emission of longwave radiation from the surface can cause a shallow stable inversion to form during the night, especially in rural areas and under clear skies. It is at this time of the day when low-level winds may become very strong, especially over the central Great Plains. Enhanced winds at this level create a low-level jet (LLJ) that may impact BL processes in urban environments (Klein et al. 2016; Hu et al. 2013).

The reduction of natural vegetation and replacement by man-made materials has led to drastically different surface characteristics. Urban areas typically have much higher SH fluxes because of the materials being used, greater surface area exposure across buildings and homes, and lower amounts of LH from less vegetation. A shallow convective or near-neutral layer of turbulence can occur at night arising from a small positive SH flux in urban areas (Schrijvers et al. 2015; Ryu and Baik 2012; Nunez and Oke 1977). Urban canyons reduce outgoing longwave radiation since the radiation cannot escape as easily. However, there are little shortwave radiation differences between urban and rural areas because of the numerous shadow and reflection offsets. Net radiation balances and the effect from SH of urban materials is reasonably explored, but there is less confidence in modelling LH flux. Even though the energy balance cannot be entirely observed, there is some capability in modelling anthropogenic fluxes (Sailor

2011). One example of this is the waste heat generated by buildings. There is a much wider range of emissivity values arising from the multitude of materials used in urban construction. Human desires are another factor to consider as A/C units, heating, automobiles, and a plethora of other manmade materials are what help contribute to urban areas being typically warmer than the surrounding rural regions, otherwise known as the UHI effect. Albeit basic in nature, a simple temperature difference between urban and rural environments is commonly used to quantify the UHI effect (Magee et al. 1999; Steeneveld et al. 2011; Bornstein 1968). Additionally, strong winds can advect properties of upwind urban or rural environments, such as warmer temperatures and air pollution, to their downwind neighbors (Cosgrove and Berkelhammer 2018).

Heterogeneity in surface roughness has a profound impact on the roughness sub-layer since roughness increases turbulence. Modeling turbulent flow is often a challenge in this layer because of the complexity, so research in this layer often assumes homogeneous urban canopies. Mean flow has been modeled much more than turbulent flow in this layer (Barlow and Coceal 2009), and only partially compared with measurements given the sparse observations. However, large-eddy simulation has recently started to become used more to model this turbulent flow (Wang et al. 2020; Tolias et al. 2018; Stoll et al. 2020). The structure of turbulent fluxes varies with height in this layer, which prevents it from utilizing surface layer scaling characteristics (Rotach 1999). Better representation of the overall flow and exchange with air aloft has been an output from air pollution and dispersion modelling studies (Macdonald 2000). The multitude of fluxes and heterogeneity of urban areas makes them very difficult to accurately represent and fully understand. The variety of building heights in urban environments create numerous turbulent eddies that have a wide range of spatial and temporal scales. The proximity of

buildings to each other and their relative heights are important for turbulence calculations in these areas. Past studies show the importance in understanding these dynamics when looking at energy budgets between buildings (Salamanca et al. 2009).

Even given these advances in modeling over an urban environment, observations are an essential component needed to study the atmosphere above urban environments. Doppler lidar is sometimes used to get profiles of urban areas but difficulties arise with obstructions from buildings or when clouds are prevalent (Barlow et al. 2011). Furthermore, it is challenging to gain permission to erect data collection towers, preexisting data collection may not be in the most desired locations, and challenges exist launching radiosondes and tethered balloons in urban areas.

Urban and rural environments both affect the BL in different ways, but the urban boundary layer (UBL) is the primary focus of this study given its complexity, importance to public health through heat stress and air pollution, and the location of measurements at airports with a high volume of traffic. Past research typically lacks information on the upper 90% of the UBL, especially in the mixed and residual layers (Barlow 2014). However, air quality has been a common motivation for scrutinizing changes in the UBL, particularly internationally, due to its direct health implications. The expansion of cities is important to consider when analyzing surface characteristics from neighborhood to regional scales as the heterogeneity can impact horizontal advection of heat, momentum, and other fluxes (Garratt 1990; Mahrt 2000). This is especially true when analyzing observations from one specific site in a city. When looking at urban environments on a small scale, it is important to consider the blending height, which marks the height where flow is homogeneous above, and flow below is directly related to the length

scale of heterogeneity at the surface (Wood and Mason 1991). This height is helpful to determine if the observations represent a wide area or if they are part of a local internal UBL.

The mixed and residual layers in rural and urban areas exhibit differences that arise from the characteristics of each region. The convective UBL is typically deeper than the nearby rural BL primarily because of the greater SH. The UBL height is typically defined by looking for a strong temperature inversion below 3km. However, this method may not be the most consistent with measurements across different instruments. Above this inversion the free atmosphere is considered to have no direct influence from the surface. The area of the UBL where the fluxes are roughly constant with height is considered the surface layer. Within this layer is the roughness sublayer and the inertial sublayer. The former is where buildings and trees exist, and the latter is where open air wind speeds are greatly affected by surface characteristics. The urban canopy is the atmospheric layer below the average building height and is greatly influenced by thermal properties of buildings radiative effects such as shadowing and reflection. In models, the top of the UBL is marked at the top of convection, which can be difficult to accurately represent near the surface because of the turbulence caused by buildings.

The evolution of the UBL is important because of its direct relationship with air pollution and the health of individuals in these environments (Petäjä et al. 2016; Yuval et al. 2020). Air pollution is a large umbrella term for a plethora of components of the atmosphere. One commonly studied is particulate matter with a diameter of less than 2.5 μm (PM2.5) and is very important because it penetrates the gas-exchange region of the lung (Brunekreef and Holgate 2002). PM2.5 impacts everyone regardless of concentration, and outdoor ambient levels are strongly linked with personal PM2.5 exposure (Sarnat et al. 2001). Surface PM2.5 generally peaks in the morning during rush hour traffic when the BL is still low and emissions are

increasing. Concentrations quickly decrease when the rapid mixed layer growth phase begins, indicating how important the exact timing of the rapid growth phase is. During the day when the BL is deep, pollution mixes over a deeper layer and the concentration of PM2.5 at the surface is low. A second PM2.5 spike exists when BL height decreases and emissions are large from the evening commute. An example of this cycle using AMDAR observations described later and PM2.5 obtained from EPA stations is depicted in Figure 1. This figure shows the diurnal median PM2.5 concentration and mean BL height across Dallas-Fort Worth for 08/01/19 – 07/31/20.

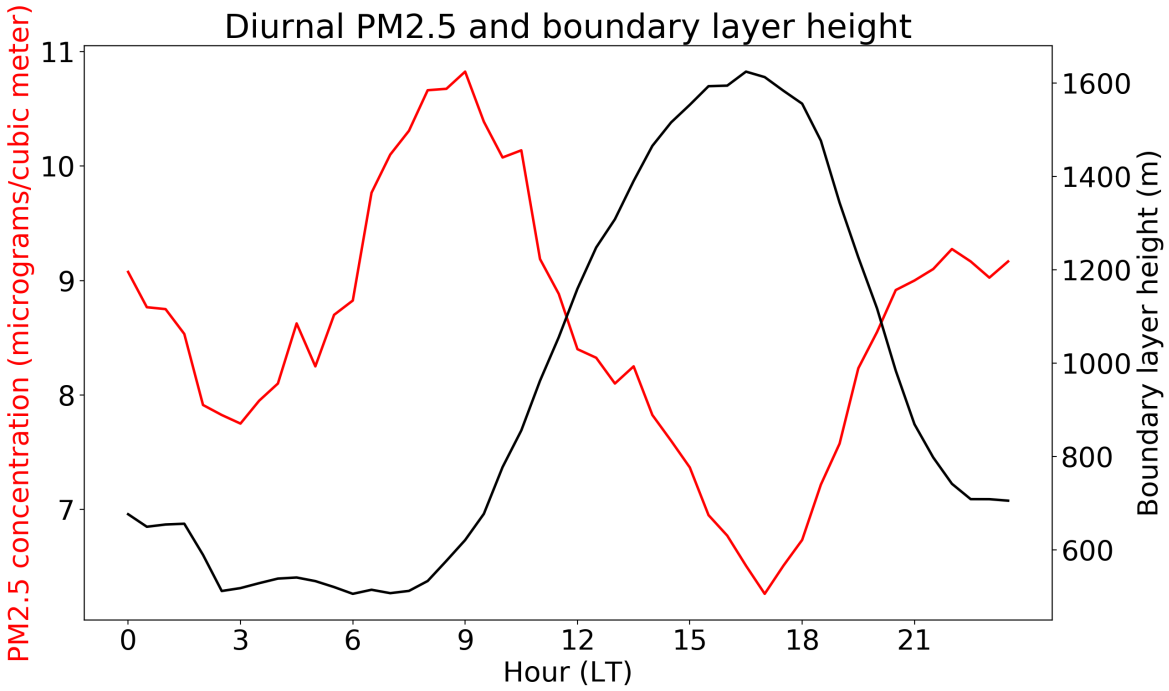

Figure 1. Median diurnal PM2.5 concentration and mean BL height across Dallas-Fort Worth for 08/01/19 – 07/31/20 using four urban EPA stations in the area.

Angevine et. al (2001) showed that the rapid mixed layer growth phase does not start immediately at sunrise, but has a lag caused by surface heating relaxing surface stability and lower atmospheric warming (between 2 m and 200 m) caused by shear-driven entrainment. This delay is called the morning transition and starts at sunrise or dawn and ends at the onset of rapid

mixed layer growth. Observations and numerical models have shown that the majority of the heating at the surface during the morning transition is not caused by incoming solar radiation but rather downward turbulent diffusion from the air (Lapworth 2006). Some of this mixing down to the surface in the stable layer reduces the stability caused by surface radiative cooling. The morning transition is used to show how long it takes to mix out the existing stable layer. Better understanding the morning transition is important because the longer the BL height remains low the more pollutants are trapped near the surface.

ii. Low-level Jet

The stable surface layer over rural terrain at night can contribute to a regional-scale LLJ that can interact with the nocturnal UBL. Nocturnal LLJs are often 100m to 500m in height from the surface and form when the nighttime surface inversion separates flow aloft from the surface friction. Stable layers form easier over rural areas and make up a larger area of the central Great Plains than urban areas alone. The LLJ is typically shallower over rural areas (Wang et al. 2007; Kallistratova and Kouznetsov 2012). Urban areas can modify the LLJ locally through processes such as enhanced mixing. The LLJ over the Great Plains partially exists from heating and cooling of the sloped terrain (Holton 1967). Holton (1967) stated that oscillations in BL winds were caused by diurnal temperature oscillations. However, this thermal forcing mechanism is not as strong as the first relationship between the LLJ and nocturnal inversions explained by Blackadar (1957). The results from Blackadar (1957) show that during the night there is a maximum in wind speed between midnight and sunrise just below 3000 ft that is typically found at the top of the residual BL. These strong winds are supergeostrophic and with high amounts of wind shear because of the southerly alignment of the ageostrophic and geostrophic wind

components. The geostrophic component exists from prominent high-pressure to the east and low-pressure over the Rocky Mountains. The ageostrophic component is southerly at night but changes direction throughout the day because of thermal turbulence and the frictional force in the BL. This directional change is the strongest in the southern Great Plains. During the daytime, the winds at the surface start to increase with lower wind shear and a reduction in the stable layer. The inertial oscillation starts as soon as the daytime mixing is diminished and decoupling with the surface starts to occur.

Using rawinsonde observations from 1994-1996, Whiteman et al. (1997) found the maximum occurrence of a LLJ to be near 37°N, 98°W, approximately 300 miles north of DFW. The LLJ was found between 300 m and 600 m above ground level and peaked around 02:00 local time. Southerly LLJs can occur year-round but are most frequent during the summer. Northerly jets can also occur year-round but are often associated with cold air outbreaks. The daily oscillation in the winds is important for creating the wind maxima between the nighttime and daytime jet frequency, which relates back to the inertial oscillation theory proposed by Blackadar (1957).

Given the relative common occurrence of LLJ in the central Plains, Klein et al. (2016) looked at the nocturnal LLJ and its relationship with the UBL in Oklahoma City. A strong LLJ led to greater nocturnal mechanical turbulence, which is important for the vertical movement of pollutant molecules. Additional thermally-driven turbulence may also exist from positive SH flux in the UBL. It was found that stronger LLJs occurred when there was stronger turbulence and weaker inversions at night. These strong LLJs were linked with greater wind speeds from the previous daytime BL, suggesting that the geostrophic forcing was also stronger. However, when there was a stronger LLJ compared to the wind speed from the previous daytime BL, geostrophic

forcing was relatively weak and surface inversions were able to form at night because of lower turbulent mixing. Barlow et al. (2015) also showed that jets in rural areas can have a significant impact on thermally generated turbulence in urban areas, especially during strong UHIs.

2. Methods

a. Data

The primary data source for this project is from the AMDAR program created by the World Meteorological Organization (WMO) (World Meteorological Organization 2017). Observations of the atmosphere include air temperature, wind speed and direction, and pressure. Additional information includes eddy dissipation rate (turbulence), latitude, longitude, time, icing indication, departure and destination airport, aircraft roll number, and flight number. Measurements during take-off and landing capture BL properties. As of November 2016, there are 40 participating airlines across 11 countries that provide approximately 700,000 observations per day. Although the number of profiles far exceed the twice-daily weather balloon launches, the timing of each profile is limited to aircraft flight patterns and frequencies. AMDAR has noticeably fewer observations during the nighttime hours due to fewer overnight flights. Under the Quality Management System, the expected uncertainty for air temperature is around 0.5 K, 2 – 3 m/s for wind speed, and 3.5 – 4 hPa for barometric pressure. One past study found the root-mean square differences between AMDAR and nearby radiosondes for over 54 U.S. airports to be 1.16 – 1.52 K for temperature, 0.64 – 1.25 g/kg for humidity, and 2.00 – 2.26 m/s for wind speed at pressure levels greater than 850hPa (Zhang et al. 2019). The overall impacts of this program and its specific uses in operational forecasting are shown by various technical reports

(World Meteorological Organization 2014, 2015, 2018). Given the high resolution sampling, a plethora of publications exist using AMDAR data (Drüe et al. 2010; Dai et al. 2014).

Surface observations come from the Automated Surface Observing Systems (ASOS) program, which is a collaboration between the National Weather Service, Federal Aviation Administration, and the Department of Defense. Taking observations every minute, the network uses the most modern weather sensors to give surface observations across the nation. There are about 20 stations in and around Dallas-Fort Worth. Each station is set up to report the sky condition, visibility, present weather, pressure, temperature, wind, precipitation, and changes for each of the variables. Quality control is performed for these instruments on three scales: on site, at a local Weather Forecast Office, and nationwide on all stations. Although limitations exist (Guttman and Baker 1996; An et al. 2019), especially with respect to cloud detection, these stations are used for surface observations. These surface observations are helpful for diagnosing any severe weather that may not be readily apparent in the AMDAR profiles, such as cloud obstructions.

Ground based radiometer and ceilometer backscatter measurements have continuous coverage and are relatively accurate but have limitations, such as being strongly affected by clouds. Ceilometers have limited areal coverage which brings up errors when skies are heterogenous (Wagner and Kleiss 2016). However, larger errors exist when using ceilometers to detect upper-level clouds, which are diurnally and seasonally dependent.

Kotthaus and Grimmond (2018a) compared lidars and ceilometers with AMDAR data to determine BL heights and classifications. The best agreement was found during the afternoon when the bulk of the BL was from the mixed layer. Noise from the AMDAR-generated inversion heights is ultimately what provided the most amount of variability in the overall statistics

computed. Temperature inversions exist above the ceilometer mixed layer height during the night and morning transition, which can cause inaccurate BL detection. However, the aerosol layer from the residual layer is tracked by the ceilometer and generally agrees with AMDAR inversion heights. Clear-sky days had the best agreement between the two instruments. Aerosols were used to show mixing during cloud-free conditions, but uncertainty arises when using attenuated backscatter profiles with cloudy conditions. The top of the BL was classified by a decrease in humidity, enhanced turbulence, and a clear temperature inversion.

Kotthaus and Grimmond (2018b) also performed a long-term analysis (2011 – 2016 in London) using the aforementioned instrumentation to show that most of the variability in the BL related to day-length (lower in the winter), cloud cover, and cloud type. The morning transition had a median value of 92 m/hr for stratiform clouds, 212 m/hr for clear nights followed by a day with convective clouds, and an overall average of 174 m/hr. The observations showed the morning transition to predominately be about 2 hours after sunrise and is most strongly related to the length of the day. The stratiform clouds were typically associated with a lower amplitude in the diurnal cycle and the convective clouds were found to be 2.5 times more likely during the summer than the winter. Mixed layer height was directly related to the frequency of the cloud types for the period analyzed, showing the significance in utilizing cloud cover, cloud type, and cloud base height. When compared with past studies (Pal and Haeffelin 2015), this study emphasized that looking at the nocturnal BL is important to approximate the onset time of the morning transition based on mixed layer height. The timing of the evening transition is generally more variable than the morning transition, arising from differences in the depth of the convective mixed layer. A significant amount of pollution can create a more stable BL that may lead to restricted mixed layer growth, which would increase the amount of pollution near the surface.

This creates a positive feedback loop that can significantly impact the health of individuals living in these areas (Petäjä et al. 2016).

b. UBL characteristics

Diagnosing UBL characteristics in Dallas-Fort Worth is the focus of this study using the relatively frequent AMDAR profiles. The AMDAR data used in this study consists of temperature and wind profiles from both the Dallas-Fort Worth International Airport (DFW) and the Dallas Love Field Airport (DAL) from 2010 to 2020. Both airports have different amounts of observations but tend to have more profiles in recent years. Data from nearby ASOS stations can be used to create a more thorough understanding of the spatial distribution across the city and characterize the UHI intensity. An example is shown in Figure 2 with an UHI intensity of 3.28°C over 25 miles between DAL and Mid-Way Regional Airport (JWY) on 06/28/19 at 12:00UTC.

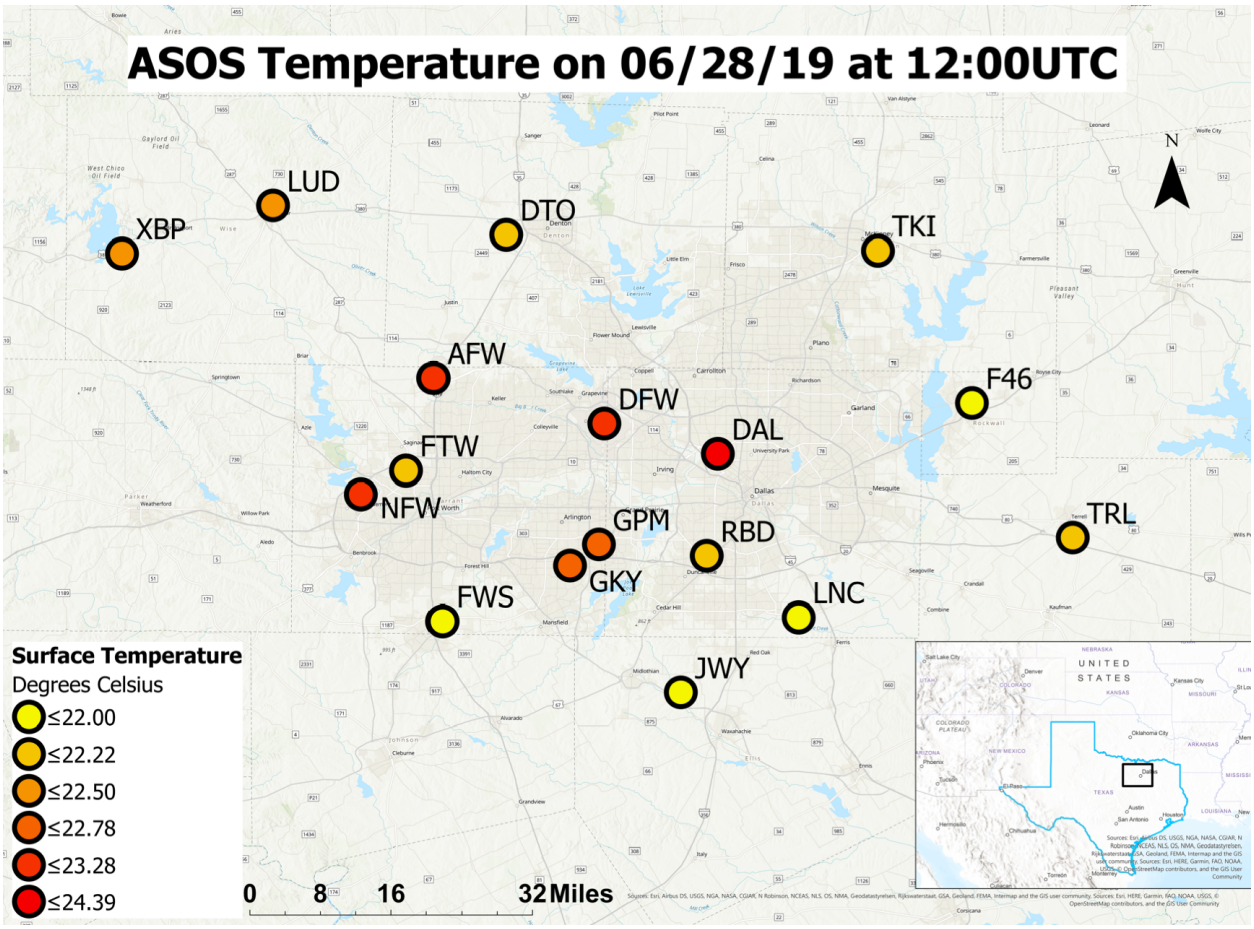

Figure 2. ASOS temperature across the Dallas-Fort Worth area on 06/28/19 at 12:00UTC. Surface conditions were clear with 5mph S-ly winds at DAL. The locator map shows the area of focus (black box) in relationship to the southern Great Plains.

Given the inconsistent nature of aircraft flight times and sampling levels, data is standardized to partially offset the significantly more observations during the day than at night. All profiles are separated into half-hourly bins and then averaged to give 48 profiles for each day. Figure 3 shows the percent occurrence of a vertical profile of temperature broken up by season in the half-hourly times around dawn (winter: December-February, DJF; spring: March-May, MAM; summer: June-August, JJA; fall: September-November, SON). Starting at dawn there is a vertical profile of temperature >90% of the time. While there are relatively less profiles prior to dawn, there are observations that can be used to analyze diurnal BL height evolutions.

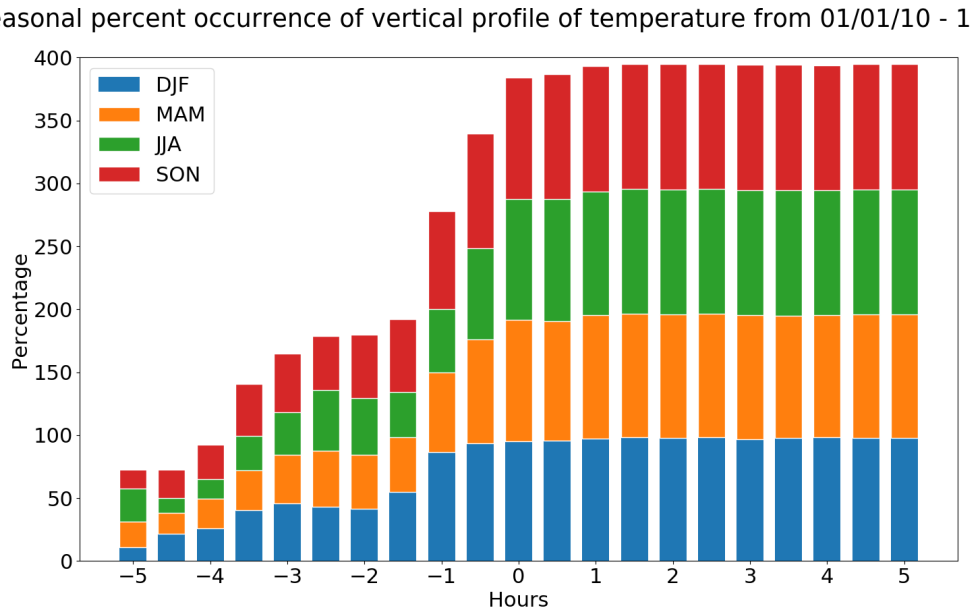

Figure 3. Percent occurrence of a vertical profile of temperature with respect to dawn for 2010 to 2020.

Interpolation is also done in the vertical dimension to facilitate better comparison between profiles. Heights are fixed to 20-meter intervals between 200m and 3000m. This vertical grid is used assuming the profiles within each half-hour interval is the same. It is done to increase the resolution between levels. This regular grid also makes it easier for calculations because the distance between each level is the same. A smaller distance between each of the levels would have a greater chance in bringing forwards larger errors in the calculations. Although the surface layer provides important information when looking at small-scale UBL dynamics, consistent and reliable data from AMDAR lacks in the lowest levels of the atmosphere. The heights listed from AMDAR are height above sea level, so no observations exist below the area's elevation of 180m.

After each of the half-hour profiles are created, they are averaged together between DFW and DAL. This is done with all the recorded properties of the atmosphere. The airports are ~11

miles apart from each other, so it is assumed that the differences between them are insignificant for the scope of this study. This was confirmed by seeing only small changes in vertical profiles of temperature and wind speed between DFW and DAL, especially further from the surface. ASOS data is used for the surface observations and even though the ASOS stations have much more consistent observations than the AMDAR data, there are still some missing observations for these stations. However, missing ASOS primarily comes from rural stations, which are not used in this analysis. It is the combination of these two sets of data for DFW and DAL that is used to understand the UBL in Dallas-Fort Worth.

c. Determining BL depth

Quantifying BL height is not trivial and can be sensitive to which method is used. Temperature gradients below 3000m can be used to determine both surface inversions and temperature inversions aloft. However, there are several issues that can occur. For example, a strong capping inversion may not exist in the summer. The nocturnal BL is also ill-defined when solely using temperature gradients, especially if there is an isothermal atmosphere. Because wind speed profiles are also provided by AMDAR, a more robust BL height detection is computed using the bulk Richardson number (Ri_b). The Ri_b method marks the BL height where the Ri_b crosses a set threshold (Ri_{bc}) based on a calculation using the potential temperature and wind speed at a given height. The Ri_b formulation was first utilized by Hanna (1969) and most recently updated by Vogelezang and Holtslag (1996) to work better with higher wind speeds and turbulence caused by surface friction under neutral conditions. Their revised formulation is written as

$$Ri_b = \frac{(g/\theta_{vs})(\theta_{vz}-\theta_{vs})(z-z_s)}{(u_z-u_s)^2+(v_z-v_s)^2+100{u_*}^2}, \quad (1)$$

where z is the height of the observation, z_s is the height of the lower boundary (often the top of the surface layer), θ_{vz}, u_z, and v_z are the virtual potential temperature, u-wind speed, and v-wind speed components, respectively, at height z. θ_{vs}, u_s, and v_s are the virtual potential temperature, u-wind speed, and v-wind speed components, respectively, at height z_s. u_* is the friction velocity and is assumed to be 1 because of what was used by Zhang et al. (2014). While friction velocity is commonly applied to motion near the ground, it is widely used in the Ri_b formulation in BL studies. Virtual potential temperature is replaced by potential temperature in Eq. 1 because few and inaccurate humidity measurements can lead to highly variable estimates in BL height. Ri_b is commonly used is numerical models because of its reliability for different stability conditions. Ri_b is not perfect because it is a better proxy for determining dynamically unstable parts of the lower atmosphere instead of specifically determining BL height. This means that the top of a nocturnal surface inversion may not be accurately detected, especially if there is a prominent residual layer, which brings forward the use of various Ri_{bc}.

The optimal Ri_{bc} used to mark the top of the BL can be anywhere from 0.15 to 1.0 but is more commonly between 0.25 and 0.5. Zhang et al. (2014) found an optimal Ri_{bc} of 0.24 for a strongly stable BL, 0.31 for a weakly stable BL, and 0.39 for an unstable BL. These optimal values were found by performing linear regression on graphs of the numerator vs. the denominator of Eq (1). The Ri_b method works well for quantifying BL height on large data sets. A Ri_{bc} of 0.25 best characterized the data and is the most commonly used threshold (Seidel et al. 2012). Seasonal variability in BL heights was found to be positively correlated with 500 hPa heights and surface temperatures. Different Ri_{bc} thresholds have a slight impact on stable and convective BLs but have more variable results for near-neutral BLs because of the large variation

in Ri_b near the surface when using AMDAR data (Zhang et al. 2020). More arid areas tend to have greater maximums in BL height because of more SH, which is important to consider when comparing results from the analysis herein to others. Drier soils may also lead to greater radiative surface cooling at night and lower minimums in BL height. The diurnal range of BL height is greater for clearer skies and is more pronounced during the spring and summer. Combining these results with past studies, this study uses a threshold of 0.25 because of the importance in analyzing dynamics of the UBL around dawn from a large data set.

Profiles are randomly sampled, such as in Figure 4, to qualitatively determine the overall accuracy of the method to detect BL heights. This figure shows that the Ri_b method works well when compared with temperature and wind profiles during the morning when the rapid mixed layer is developing. Using the Ri_b method instead of just temperature profiles adds to the accuracy of the overall detection, especially during the summer when the top of the BL does not have a clear capping inversion. Gradients in humidity could also contribute to BL detection, but there are few humidity measurements, so they are omitted from this study.

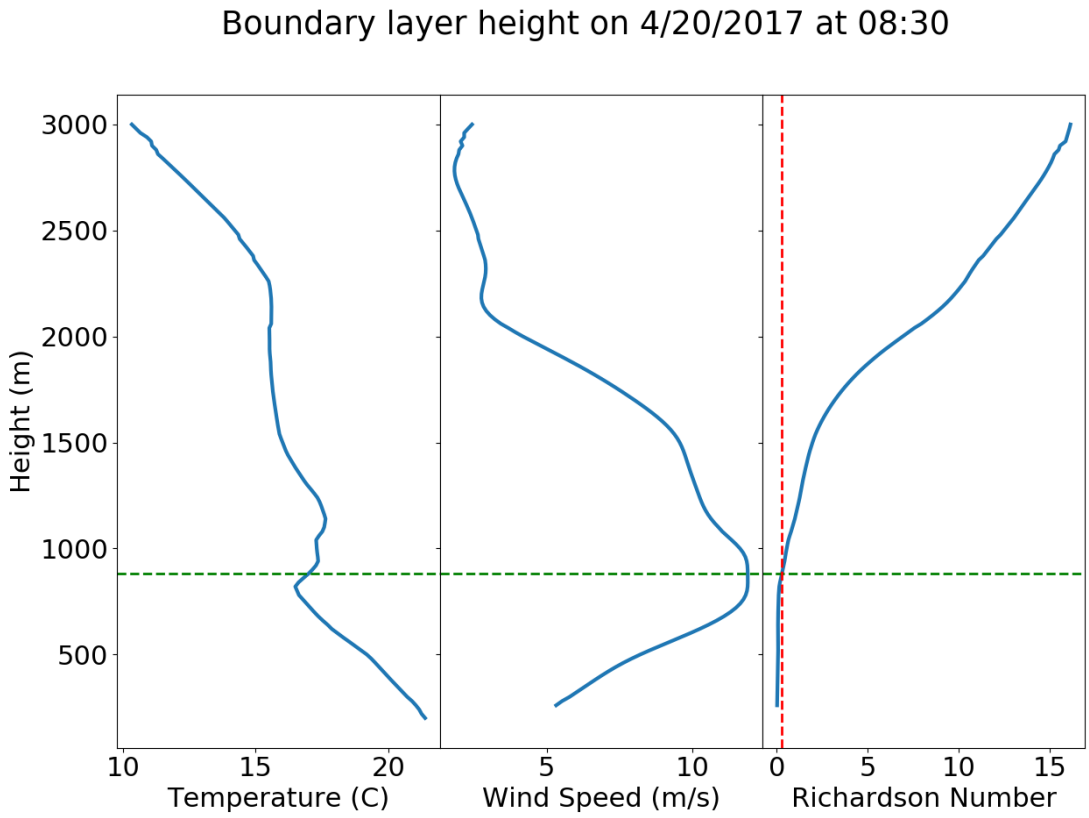

Figure 4. Profiles of temperature (left), wind speed (middle), and Richardson number (right) with a BL height of 880m (green dashed horizontal line) determined by a Richardson number threshold of 0.25 (red dashed vertical line).

d. Determining time of morning transition

After finding BL height for each half hour interval, the next step is to identify when the morning transition occurs. The morning transition can be identified using changes in near-surface wind, near-surface heat flux sign, or the moment when convection reaches 200 m (Halios and Barlow 2018; Lapworth 2006; Angevine et al. 2001). Changes in near-surface wind are difficult to determine if there are no accurate sensors, and surface heterogeneity in urban environments makes these measurements even more complex. Negative to positive SH flux doesn't work for this study because of no explicit SH measurement. There could also be positive SH flux at night from excess heat in the city. Using a threshold of 200 m is not applicable since

the BL may already be greater than 200 m at night. Additionally, 200 m was used arbitrarily because it was the height of the tower used in the study by Angevine et al. (2001). The morning transition in this analysis starts at dawn and ends at the onset of rapid mixed layer growth.

A break point is found using the intersection of two linear regressed lines on the diurnal BL height to approximate the end of the morning transition. The algorithm takes a specified number of breakpoints (2 in this study) and goes through every possible breakpoint combination to find where the mean squared error of the best-fit lines with respect to the actual function (the diurnal BL height) is minimized. An example of this method on the mean BL height for all seasons is shown in Figure 5. Also known as change point detection, break point analysis is commonly used to detect shifts in the climate through various techniques (Reeves et al. 2007; Lund et al. 2007).

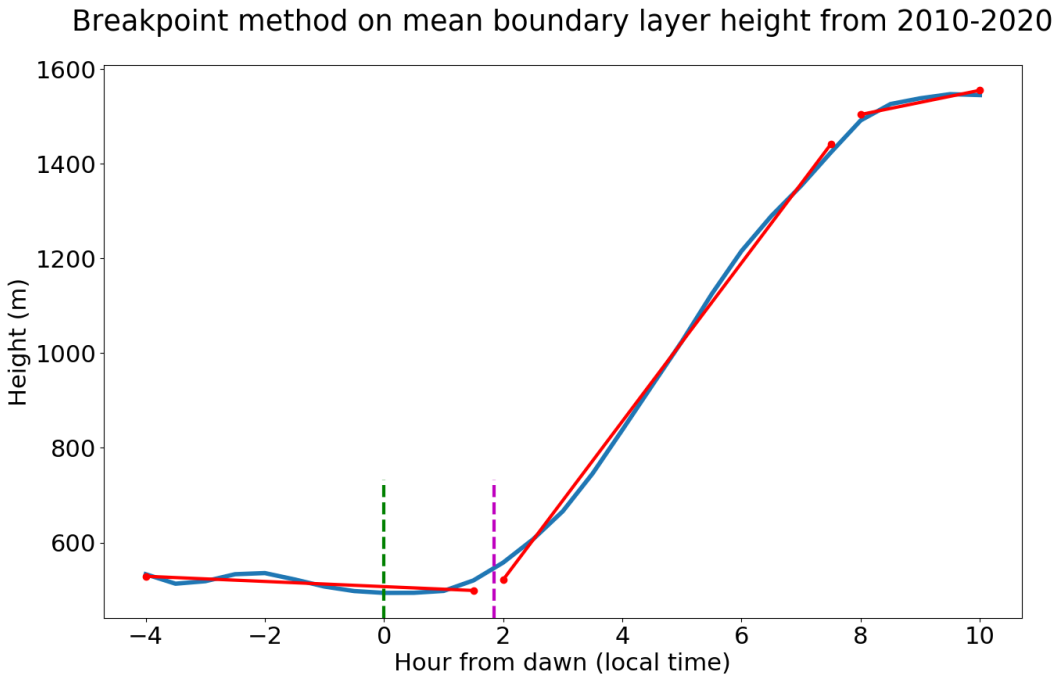

Figure 5. Breakpoint method using the mean mixed layer height a Ri_{bc} of 0.25. The green dashed vertical line represents dawn, and the purple dashed vertical line represents the end of the morning transition, giving a total duration of 1.852 hours.

Using a larger Ri_{bc} leads to greater BL heights because Ri_b increases with height as potential temperature increases and wind speed above the local maximum decreases. Computing the morning transition on the mean BL height (as in Figure 5) with a Ri_{bc} of 0.30 gives a duration of 1.839 hours (shown in Figure A.1) and a Ri_{bc} of 0.20 gives a duration of 1.853 hours. This gives a robust result showing that the morning transition duration doesn't change much from using 0.20 to 0.30 for Ri_{bc}, which is the most used range. Nonetheless, 0.25 will be used from here on out.

e. Wind speed

Other than the profiles of wind speed used in the Ri_b calculations, the wind speed maximum around dawn is used to determine relationships with the morning transition. Southerly LLJs are the prevailing wind pattern in the Dallas-Fort Worth area and are selected to compare to the morning transition. This is done to eliminate northerly LLJs that occur behind cold air outbreaks, especially during the winter months when the baroclinic zone is pushed further south. To estimate the strength of the LLJ around dawn, the average of the greatest wind speed below 800 m between one hour before dawn and one hour after dawn is used. Wind speed maxima at fixed heights were analyzed but lacked in accurately picking up the peak of the LLJ, especially for periods with fewer observations. Wind speed maxima are used instead of the LLJ classification from Bonner (1968) because the averaging done with the AMDAR profiles reduce the wind speed gradients, which may prevent a LLJ from being detected.

f. Quality control

To ensure that the results are a product of physical processes instead of being an artifact of the data or methods used, quality control is performed on the data set. Using a 7-value moving average, BL heights greater than one and a half standard deviations above or below the mean are removed. If one missing BL height is surrounded by two BL height values, then the missing height is replaced with the average of the two nearby values. Gap filling is also performed for two consecutive missing BL heights surrounded by one BL height on each side. Instead of strictly being replaced by the mean of the outer values, each of the two missing BL heights are replaced by a value linearly weighted towards the nearest BL height.

To exclude days with transient weather events and top-down forcings caused by cloudy conditions that impact mixed layer height more than local effects, days when cloud cover is five or more oktas are excluded. This is done to exclude broken or overcast skies. Clouds remain a strong uncertainty based on their infiltration of UBL structure (Shepherd 2005). During a cloudy night, a separate turbulent layer exists just beneath the cloud base and is caused by cloud top cooling. This is often referred to as an upside-down convective BL because cold air parcels will sink down to the surface, which forces rising parcels because of mass continuity. While these BL clouds are prevalent over the ocean, they also exist during post-frontal conditions. More entrainment is likely as time goes on because of the increased mixing. This forcing causes greater nocturnal BL depths and lower daytime BL depths compared to the cloud-free atmosphere. Lower daytime BL depths are caused by less mixing and subsidence. This flatter diurnal BL height would bring added challenges in detecting the end of the morning transition. Past research also shows that BL height is more difficult to determine when a frontal system passes with precipitation or when there are blustery winds (Haman et al. 2012). This problem is

more common when attempting to use aerosols to quantify BL depth, but major synoptic events are thrown out in this study since they are dominated by large-scale forcing and unrelated to local forcing in the UBL.

Cloud oktas are recorded by ASOS stations and have noticeably more consistent observations than the AMDAR data. Assuming the difference in cloud coverage between DFW and DAL is negligible, the values recorded at each airport are averaged and rounded to give an estimate of the cloud cover for each half-hour profile. If only one value is recorded between the two airports, then that value is used in the data set. If there is more than a four okta difference between the airports, then both values are removed from the analysis. While cloud cover may change more than temperature or wind speed, these filters are necessary for the breakpoint to be accurate and controlled.

3. Results

To gain a baseline understanding of the region, a climatology of the UBL is computed. The DFW and DAL ASOS stations have relatively frequent observations, but there is more missing data for wind and cloud observations. The lack of cloud coverage caused by missing ASOS cloud data from individual stations brings forward the motivation behind using a combination of observations from DFW and DAL. Albeit with a coarse resolution, satellite data, such as from National Aeronautics and Space Administration's (NASA) Moderate Resolution Imaging Spectroradiometer's Cloud Mask product, could have also been used as an additional proxy in the analysis. However, this product only provides information about the cloud top and the base of the cloud is most important in analyzing BL dynamics (i.e., top-down radiative cooling for stratus). NASA's Modern-Era Retrospective analysis for Research and Applications

Version 2 (MERRA-2) reanalysis has cloud fraction information that could be helpful in future studies.

The distribution of BL heights at dawn filtered by cloud oktas less than five is shown in Figure 6 and reveals that most heights are between 300 – 700 m. As expected, deeper heights tend to occur during the summer months and lower heights during the winter. There are close to no days with heights less than 300 m in the summer but around 115 days during the winter months. Comparing the transition seasons, they mostly seem to match up above 500 m except for spring months generally having more frequent depths greater than 800 m. The greater increase of SH in the summer leads to more growth of the BL.

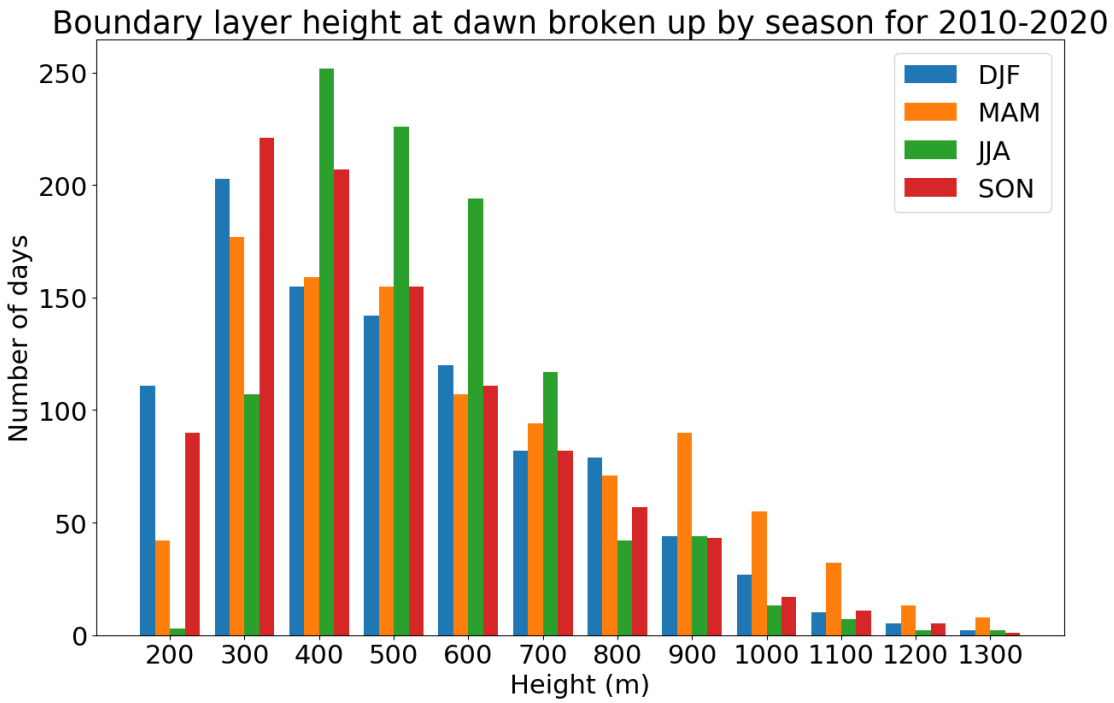

Figure 6. BL height (m) at dawn by season for 2010-2020.

To investigate the impact of wind on BL height and morning transition duration, the average diurnal cycle conditioned by the greatest southerly wind speed below 800 m at dawn is

found. This is shown in Figure 7 and is broken down by season to bring forth striking differences. These 5 m/s wind bins are chosen to allow ample observations in each category. Using bins too small or too broad (i.e., 20+ m/s) brings forward additional variability from a low sample size. The number of observations used in each diurnal BL height is conditioned by the number of observations at dawn and is noted in the legend. For example, there are 16 observations at dawn with wind speeds greater than 15+ m/s during the winter, but this number reduces as the time before dawn increases. This is an explanation for the added variability and spike around 5 hours before dawn. There are noticeably more observations in the summer than the winter. This is a result of the wind being filtered by only the southerly component. Northerly LLJs are more likely to occur during the winter months, which limits the amount of southerly LLJs analyzed. Additional cloud cover also exists during the winter.

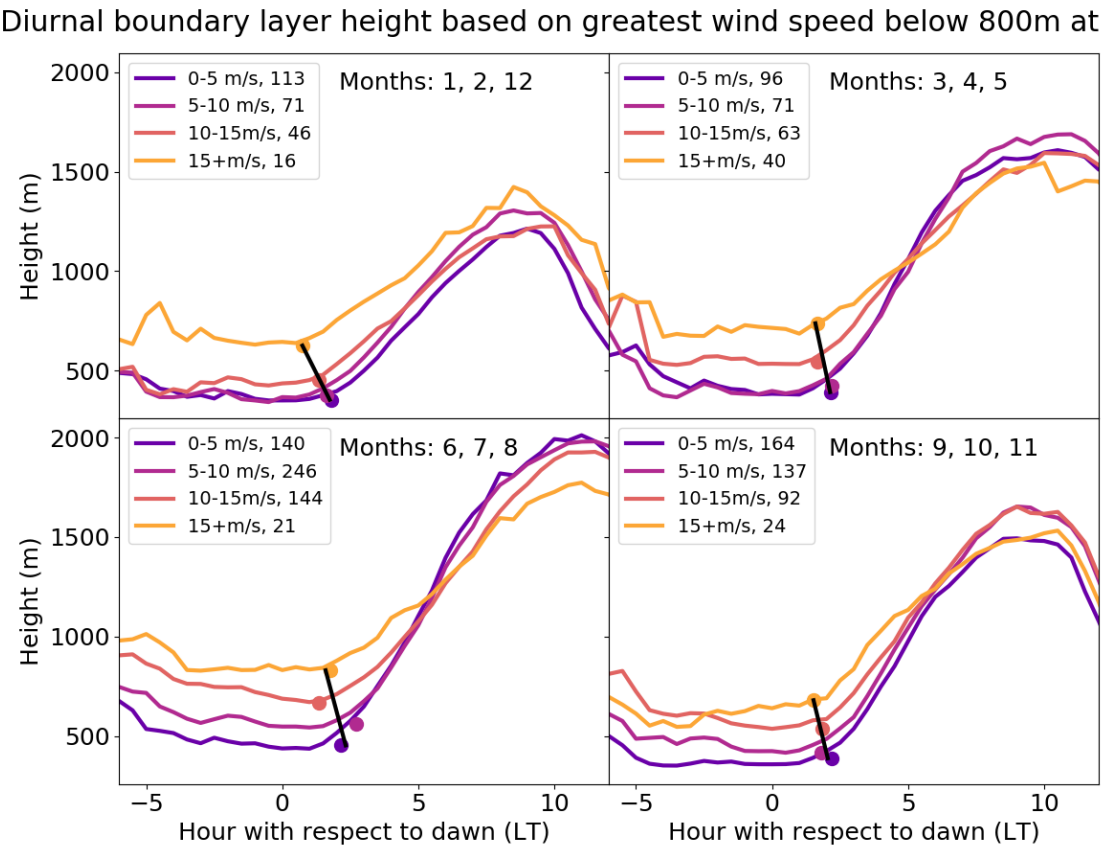

Figure 7. Diurnal BL height (m) in each season averaged using the greatest southerly wind speed below 800 m at dawn. Bin ranges and samples per bin at dawn are indicated in the legend. The morning transition from the breakpoint method is indicated with color-filled circles and with a best-fit line.

The distribution of BL heights when winds are less than 5 m/s from Figure 7 is shown by the boxplot in Figure 8. The distribution of the BL heights increases as the time after dawn increases and starts to decrease when the BL height begins to decrease in the late afternoon. This large spread during the night is explained by using the Ri_b calculation at night when a prominent residual layer may exist. The interquartile ranges at night are relatively consistent across each season, especially between four hours before dawn and dawn.

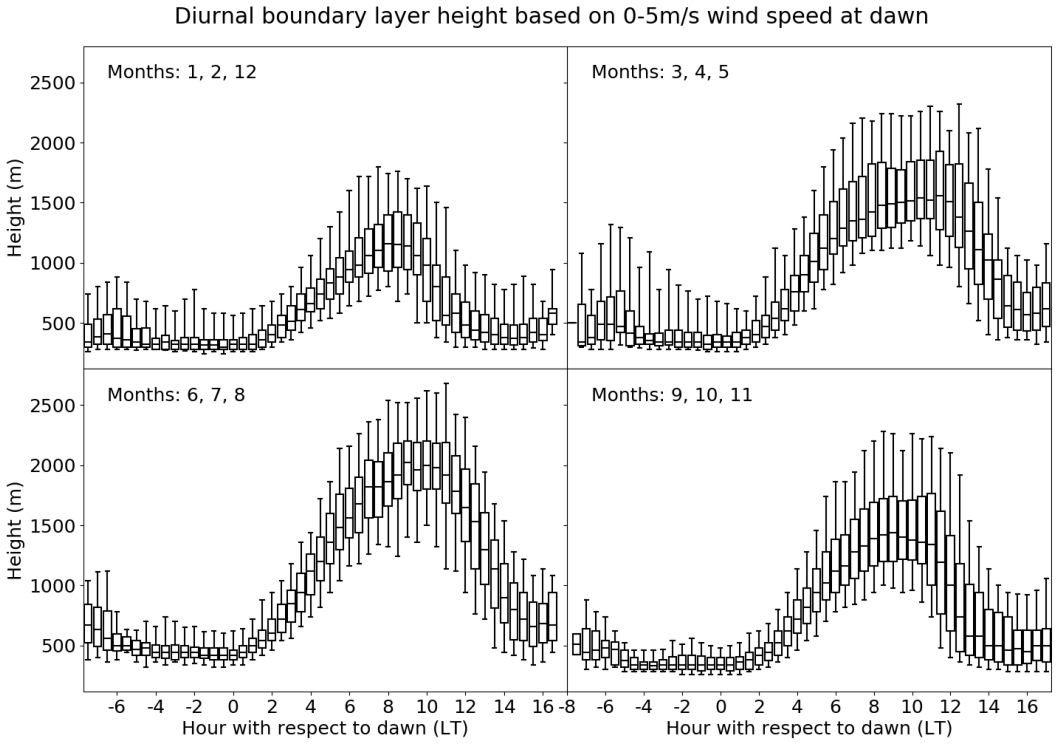

Figure 8. Distribution of diurnal BL height (m) for 0-5 m/s winds at dawn in each season.

Table 1 provides the morning transition duration for the wind bin in each season in Figure 7. In each season, greater wind speeds generally lead to shorter morning transitions, as also highlighted by the negative slope in Figure 7. Shorter morning transitions are evident during the winter with generally longer transitions in the summer. The average duration is 1.784 hrs, which is 0.07 hrs away from the duration on the mean diurnal BL height. This shows that the breakpoint method is consistent within itself.

Table 1. Morning transition duration for each season in Figure 7.

Wind bin	Winter (12, 1, 2)	Spring (3, 4, 5)	Summer (6, 7, 8)	Fall (9, 10, 11)
0-5 m/s	1.81 hrs	2.15 hrs	2.17 hrs	2.18 hrs
5-10 m/s	1.61 hrs	2.21 hrs	2.70 hrs	1.81 hrs
10-15 m/s	1.34 hrs	1.67 hrs	1.33 hrs	1.85 hrs
15+ m/s	0.76 hrs	1.68 hrs	1.75 hrs	1.51 hrs

The start and end time of the diurnal BL height used in the breakpoint algorithm impacts the average morning transition duration, as shown in Table 2. An ending window later than eleven hours after dawn will pick up more of the decreasing BL height and start of the residual layer, which will cause a less steep best-fit line for the rapid mixed layer growth phase and a shorter duration. Too late of a window end will eventually cause an error as too much of the residual layer will be picked up and the intersection of the best-fit lines will be outside the expected range of zero to five hours. The same is true for too early of a window start picking up too much of the nocturnal residual layer, which would give a steeper nocturnal BL height best-fit line and shorter duration. Although the slopes in Figure 7 are qualitatively useful to show trends between different wind bins, specific values become harder to interpret as some of the lines become nearly vertical (mainly for March, April, May), which impacts the averages in Table 2. Overall, the differences in duration are small and show that the window used for the breakpoint method does not significantly influence the results.

Table 2. Morning transition duration and slope as a function of the start and end time used in the breakpoint algorithm.

Window start	Window end	Duration (hrs)	Slope (m/hr)
-4	9	1.869	-1696
-4	9.5	1.824	-777
-4	10	1.784	-495
-4	10.5	1.847	-1045
-4	11	1.823	-1841
-5	10	1.695	-1516
-4.5	10	1.768	-972
-4	10	1.784	-495
-3.5	10	1.783	-528
-3	10	1.767	-525

After looking at the evolution of BL height, the evolution of wind speed is important to analyze. As shown in Figure 9, rapid mixed layer growth causes a sharp decrease in winds, mainly for wind speeds >10 m/s. Weaker winds are more frequent than stronger winds. The most frequent winds greater than 15+ m/s occur during the spring, but stronger average wind speeds greater than 15+ m/s exist during the winter.

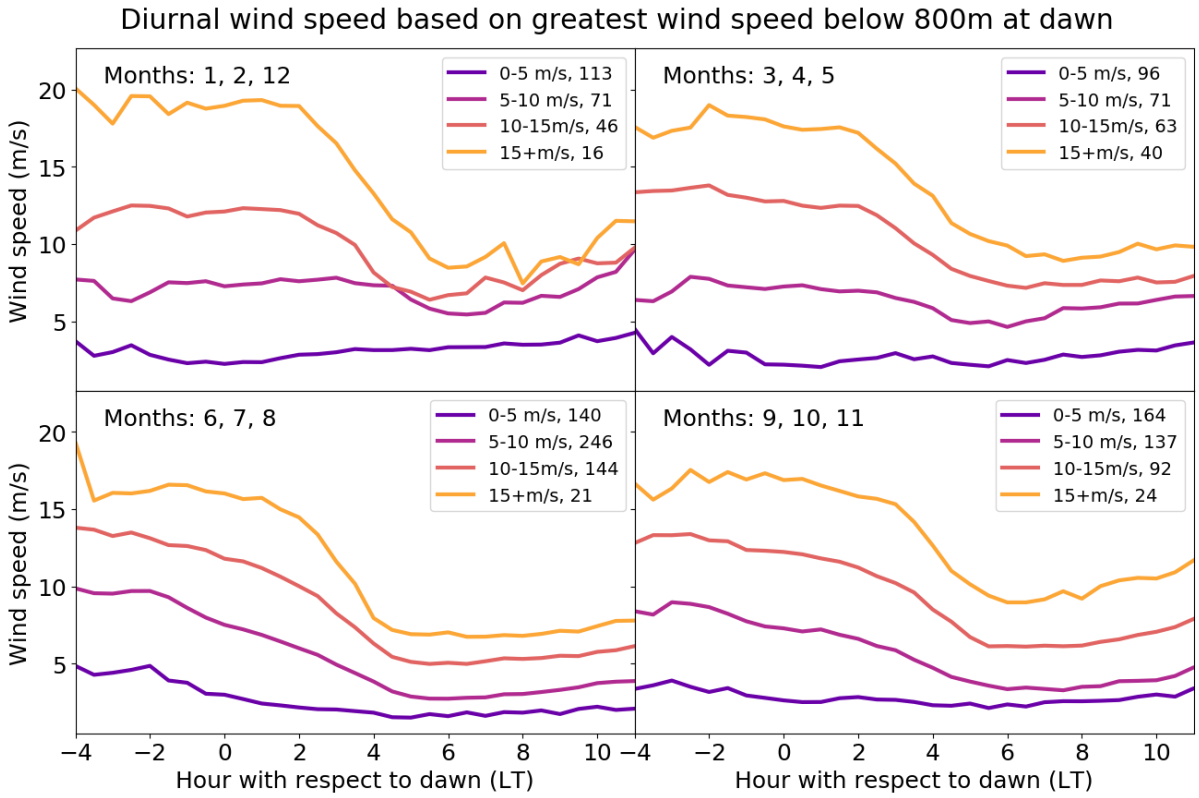

Figure 9. Same as Figure 7 but for wind speed (m/s).

Other differences become evident when looking at the average temperature and wind profile at dawn within each season, as shown in Figure 10. Using narrower wind bins makes it easier to determine when a profile switches from being stable to isothermal, as shown in Figure 11. Dawn is selected because that is when the morning transition starts. Some profiles have a

lower number of observations used in the mean profile, but relationships are still able to be deduced. The crossover from stable to isothermal tends to happen around 15+ m/s for the winter, 9-12 m/s for the spring, 0-3 m/s for the summer, and 12-15 m/s for the spring. The spring and fall profiles generally match up except for 15+ m/s, which could be an outlier, perhaps from a LLJ ahead of a cold front.

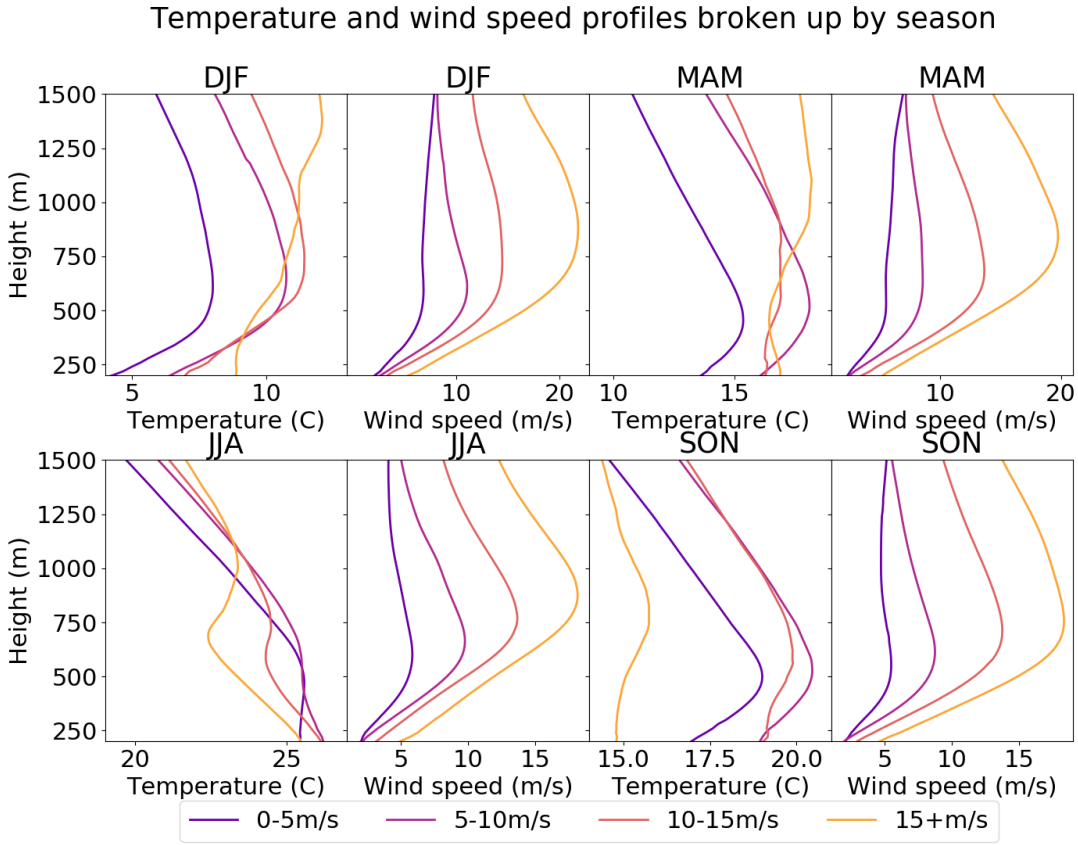

Figure 10. Average temperature and wind profile at dawn for each season binned every 5 m/s.

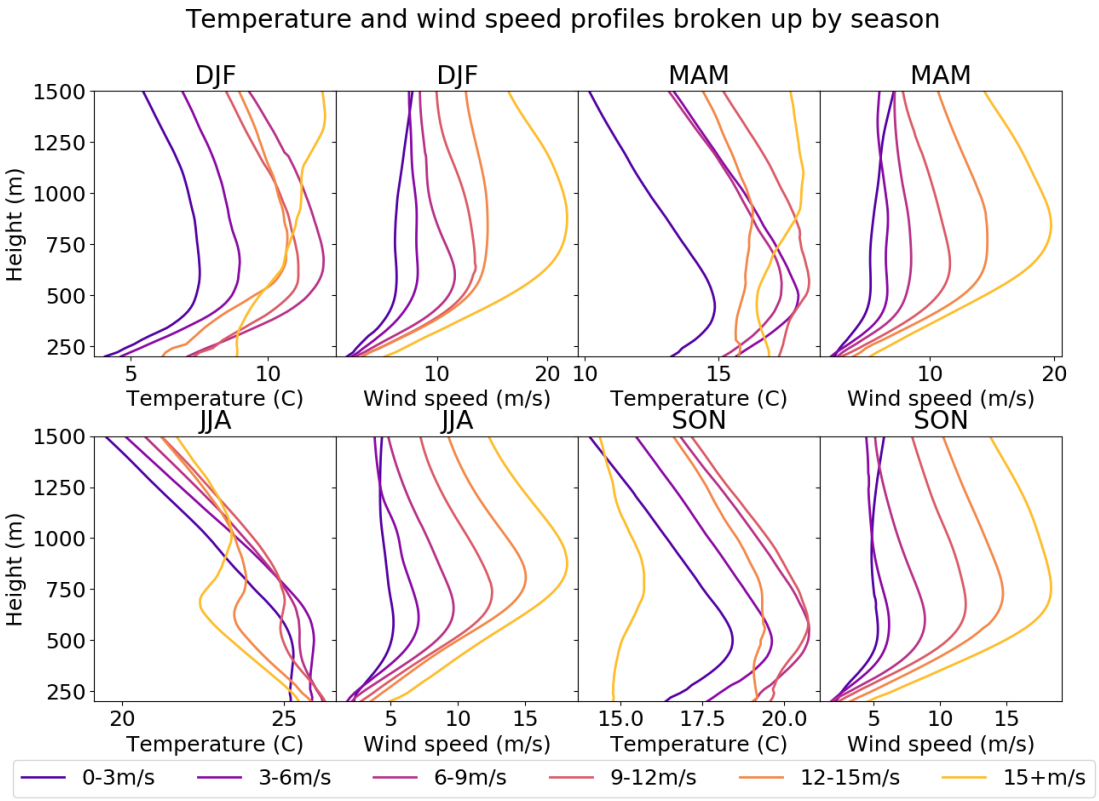

Figure 11. Same as Figure 10 but binned every 3 m/s.

The previous figures perform the breakpoint algorithm on a mean diurnal BL height evolution. While using the mean prevents analyzing the spread in the observations, the breakpoint algorithm only works when there is a full time series in the window specified. For a window of four hours before dawn to ten hours after dawn, there needs to be an observation at each half-hourly time otherwise the breakpoint algorithm will not work. This is the main drawback of performing the breakpoint algorithm on individual diurnal BL height time series' before compiling the morning transitions for each season and wind bin. Linear interpolation can be used to gap fill the missing observations, but the gaps are often too large. Performing the breakpoint algorithm on days with complete observations gives morning transitions shown in Figure 12. Filtering the results from 0 to 5 hrs gives a mean daily duration of 2.148 hrs, 0 to 3.5 hrs gives 1.937 hrs, 0 to 3 hrs gives 1.797 hrs, and 0.76 to 2.70 hrs (min. and max. from Table 1)

gives 1.845 hrs. Using a filter of 0 to 3 hrs gives a duration closest to the average duration of Table 1 of 1.784 hrs. Using the minimum and maximum values from Table 1 gives a value closest to the average duration from the mean diurnal BL height evolution (from Figure 5) of 1.852 hrs. However, these results only have 84 days used compared to the 1,484 days (defined by the number of dawn observations) used in the mean diurnal BL height evolution. In general, these results show that calculating the morning transition on diurnal BL height broken up by season yields a similar average duration to calculating the morning transition on individual days.

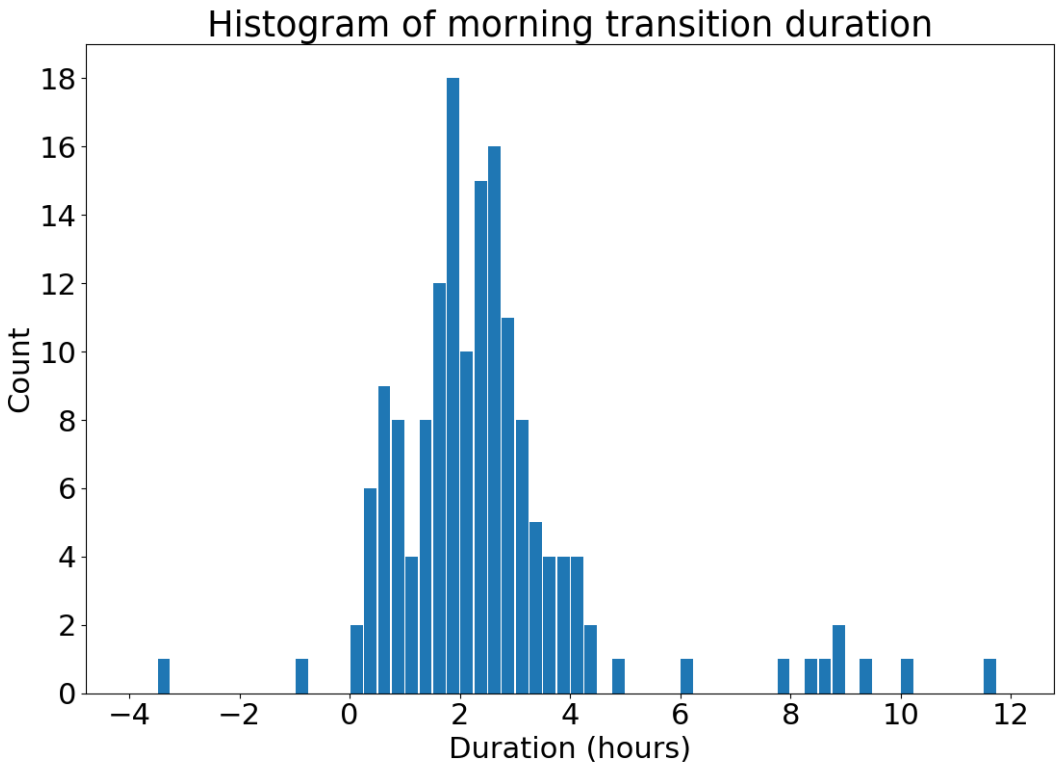

Figure 12. Distribution of morning transition durations performing the breakpoint algorithm on individual days using a window range of -4 to 10 hrs.

4. Summary and Discussion

Using the ample observations from AMDAR, characteristics of the lower atmosphere are obtained and diagnosed. In particular, the morning transition is identified and the relationship of the time of the morning transition and the wind speed at dawn is demonstrated. Determining a relationship between wind speed and the morning transition requires other factors to be controlled. Removing days with cloud oktas above four helps alleviate several issues. BL clouds may prohibit the development of a shallow stable layer and maintain a relatively well-mixed BL during the night. Since the research questions investigate the transition of a shallow stable layer into a deep, well-mixed layer, mornings with a cloudy BL are not germane to answering those questions. Clouds are also typically associated with more transient weather events, including frontal passages that can greatly disturb the lower atmosphere. Frontal passages may also come with strong low-level winds, and strong northerly winds can also be associated with clear, post-frontal conditions. Looking at past weather maps as another quality-control step shows that this simple filtering scheme works well when there are clouds or post-frontal conditions. A weak cold front without heavy cloud cover can occur, but these are not common.

After filtering by cloud coverage and wind direction, it becomes clear that the deepest BLs at dawn exist during the summer, which is expected. This shows that BL heights are at least partially correlated with surface temperature (Figure A.2 and Figure A.3). However, without observations of sensible and latent heat it is difficult to go into more detail on the role of surface forcing over the Dallas-Fort Worth area. BL heights are lower and reach their maximum earlier in the day relative to dawn in the winter than the summer, which reflects the annual cycle of radiative forcing. After observing fewer vertical profiles further before dawn, it appears variability in the mean nocturnal BL height is partially influenced by a lower number of

observations. More synoptic activity also tends to occur during the winter because the baroclinic zone is further south, which together explain the lower number of observations compared to the summer since there would be more clouds and northerly winds. Heights are lower because of less incoming solar radiation and peaks are reached earlier relative to dawn. Using 10 years of AMDAR data from 54 airports across the U.S. and ERA5, Zhang et al. (2020) observed BL heights reaching their maximum around the same local time for each season. Seidel et al. (2012) found similar results but with sparse radiosonde observations from Europe and the continental U.S. in combination with reanalysis and climate model data. Although the previous studies used low temporal resolution datasets of radiosondes (twice a day), climatological models (6-hourly), and ERA5 reanalysis (3-hourly), they are consistent with the time of maximum BL height after converting time with respect to dawn (Figure 7) to local time. Nighttime depths are greater during the summer than the winter, which contradicts Zhang et al. (2020) perhaps because they used a Ri_{bc} of 0.5. Seidel et al. (2012) also found greater BL heights during the winter, but they attributed it to climatologically greater winds during the winter. The AMDAR observations show that even in the presence of winds greater than 15 m/s, there are greater BL heights during the summer (Figure 7).

After determining seasonal BL depths conditioned on wind speed, a breakpoint method is used to determine the morning transition. There is some sensitivity to exactly how the breakpoint is determined. For instance, choosing a different starting and ending range for the breakpoint method brings forward slight differences in the morning transition duration. However, these results are relatively small and more of a byproduct of picking up a late afternoon decrease in BL height. In general, a window from four hours before dawn to ten hours after dawn is the most robust with little fluctuation in the duration with incremental changes in window start and end.

This robustness is used to show that the results are a product of wind speed instead of an artifact of the start, end, or length of the window used.

The breakpoint method is then used to examine the relationship between time of the morning transition and the wind speed at dawn. From Figure 9, the 15+ m/s wind bin has the greatest change in diurnal wind speed. The strongest wind speeds for wind bins 15+ m/s and 10-15 m/s occur in the winter. Strong wind frequency cannot be directly compared with Whiteman et al. (1997) since they included both northerly and southerly LLJs, but their average southerly jet peak speed was 19.5 m/s, which is much larger than this analysis. This is from the LLJ generally peaking around 02:00 LT, whereas this analysis looks at the strength of low-level winds at dawn, several hours after the peak in the nocturnal jet.

From Figure 10, winds greater than 10 m/s are generally associated with stable temperature profiles in the winter but are well mixed in the summer. The winter is more stable because of longer nights and strong radiational cooling, which enhances the surface temperature inversion. Temperature profiles tend to steadily transition from very stable to isothermal and then to well-mixed as the wind speed increases. The summer is the only season that shows a clear well mixed temperature profile for winds > 10 m/s, whereas the other seasons are at most isothermal for winds 15+ m/s. This suggests that strong temperature inversions, such as those in the winter, are unlikely to become well mixed in the presence of strong low-level winds. In the summer, radiative cooling is lower, especially over an urban area, and the temperature inversion is less intense, which makes it easier for the mechanically-generated turbulence associated with strong low-level winds to overcome the weaker stability near the surface. Wind speed maximum occurs at higher heights during the summer because of greater temperatures and more thermal mixing. The summer also has a steadier increase in wind speed with height than the winter. Wind

speed decreases near the surface because of additional friction caused by surface roughness. While the maximum wind speed heights here are greater than those from Whiteman et al. (1997), they are in general agreement with their findings.

5. Conclusion

The main objectives of this study are to first assess the ability of commercial aircraft observations to determine base climatological features of the lower atmosphere over Dallas-Fort Worth using AMDAR data from DFW and DAL, develop an objective method to find the time of the morning transition, and investigate the role of the low-level wind in contributing to the day-to-day variability over this urban location in the Great Plains by quantifying the relationship between the low-level winds and the time of the morning transition. With an increasing global population will come an increase in urbanization and its concomitant health risks, such as increased respiratory diseases with greater air pollutant levels. It is important to better understand urban environments because of their link with the health of individuals living in these areas.

Dallas-Fort Worth is a large metropolitan area in the central Great Plains that is free from major topographic features or coastal influences that can dominate the local forcing. There are also two busy airports in the area with ample AMDAR observations that provide sufficient profiles of the lower atmosphere. Half-hour profiles from 2010-2020 are selected to provide abundant observations over the urban environment. From these profiles of potential temperature, u-wind and v-wind speed, the BL height is computed using the Ri_b formulation from Vogelezang and Holtslag (1996) with a Ri_{bc} of 0.25. This Ri_{bc} was chosen to be consistent with past studies that determine BL height (Zhang et al. 2014; Seidel et al. 2012).

Although the location in focus is far from coastal and topographic influences, it is still prone to transient weather events. To eliminate these events and top-down forcings caused by cloudy conditions that impact mixed layer processes more than local effects, observations with cloud oktas less than five are selected. Strong northerly winds may exist immediately after the passage of a cold front, so only southerly winds are analyzed to focus on the impact from the Great Plains LLJ and not strong winds likely associated with a frontal passage. Additionally, linear gap filling is performed if there are one or two consecutive missing BL heights.

After filtering the dataset, a baseline climatology of the UBL shows heights at dawn in the summer have greater heights compared to the winter. This is likely from more incoming solar radiation and increased SH during the summer. Peak BL heights are also seen a couple hours after solar noon. Diurnal BL height time series in the summer show that BL height is deeper for greater wind speeds at dawn but become shallower in the afternoon compared to slower winds at dawn. In the winter, BL height is always deeper for greater wind speeds at dawn. Across all seasons, the strongest winds at dawn will decrease wind speed the most during the rapid mixed layer growth phase.

Using times series of BL height, the morning transition duration can be calculated, which is defined as starting at dawn and ending at the onset of rapid mixed layer growth. Past studies mark the end of the morning transition as either changes in near-surface wind, when the SH changes sign, or when the BL height reaches 200 m (Halios and Barlow 2018; Lapworth 2006; Angevine et al. 2001). Near-surface wind is difficult to obtain without accurate sensors and surface heterogeneity adds additional complexity. Changes in SH does not work for this study because of no SH measurement and the urban environment could have positive SH at night. A

BL height threshold of 200 m is too crude and invalid because the BL height is often above 200 m at night.

Because of the urban nature of the location in focus, a breakpoint algorithm using piecewise linear regression is the most reasonable approach to determine the end of the morning transition. The algorithm performs a brute-search method with every possible breakpoint combination to find where the mean squared error of the best-fit lines with respect to the diurnal BL height is minimized. Changing the window within the breakpoint algorithm causes slight departures because of picking up different parts of the decrease in BL height during the afternoon. However, these departures are small showing robustness in the breakpoint algorithm. The optimal window to use for the breakpoint algorithm is four hours before dawn to ten hours after dawn, which is shown as being the inflection point in Table 2. Similarly, changing the Ri_{bc} from 0.20 to 0.30 does not significantly affect the morning transition durations.

After eliminating upside-down convective BLs and transient weather events by removing northerly winds and cloudy skies, and after showing robustness in the breakpoint algorithm and Ri_{bc}, it becomes clear the morning transition duration is dependent on the strength of the southerly wind speed at dawn. More specifically, stronger winds lead to a shorter morning transition duration where the existing nocturnal BL is mixed out faster. Stronger winds, especially during the summer, are associated with a more well-mixed layer at dawn when the morning transition starts. This suggests that a stronger LLJ is the primary factor in leading to a shorter morning transition, quicker start of rapid mixed layer growth, and ultimately a faster mixing out of pollutants from the morning commute. This is shown using a much larger dataset than previous studies from the AMDAR program and at Dallas-Fort Worth, Texas. These

findings are paramount for those living in this urban area because of the plethora of health risks caused by high levels of air pollution.

The results are not to come without drawbacks. One drawback is the limited number of observations pre-dawn, which is manifested into averages of BL height, wind speed and temperature. The Ri_b formulation is known to have limitations during the nighttime, but most BL height detection methods have trouble detecting nocturnal BL height. This is also true for models detecting nocturnal BL height. The breakpoint algorithm only works with a full set of half-hourly observations from the start to the end of the specified window, which prevents it from being particularly useful when working with the diurnal BL from individual days instead of seasonal averages. The limited observational datasets prevent additional factors to condition by besides wind speed. For example, soil moisture, SH flux or other surface processes could also be analyzed, as well as rural measurements to compare with these urban observations.

The results from this study are only focused on the Dallas-Fort Worth area, although numerous cities in the Great Plains take part in the AMDAR program. Although farther from the strongest observed LLJs, Kansas City would be another location to focus on to see if similar results are observed, but perhaps to a lesser extent. Comparing these observations and conclusions with the Weather Research Forecast model could help solve some of the problems, such as limited pre-dawn profiles.

References

An, N., R. T. Pinker, K. Wang, E. Rogers, and Z. Zuo, 2019: Evaluation of cloud base height in the North American Regional Reanalysis using ceilometer observations. *Int. J. Climatol.*, 1–18, https://doi.org/10.1002/joc.6389.

Angevine, W. M., H. K. Baltink, and F. C. Bosveld, 2001: Observations of the morning transition of the convective boundary layer. *Boundary-Layer Meteorol.*, **101**, 209–227, https://doi.org/10.1023/A:1019264716195.

Barlow, J. F., 2014: Progress in observing and modelling the urban boundary layer. *Urban Clim.*, **10**, 216–240, https://doi.org/10.1016/j.uclim.2014.03.011.

Barlow, J. F., and O. Coceal, 2009: *A review of urban roughness sublayer turbulence*. 1–69 pp. http://research.metoffice.gov.uk/research/nwp/publications/papers/technical_reports/reports/527.pdf.

——, T. M. Dunbar, E. G. Nemitz, C. R. Wood, M. W. Gallagher, F. Davies, E. O'Connor, and R. M. Harrison, 2011: Boundary layer dynamics over London, UK, as observed using Doppler lidar during REPARTEE-II. *Atmos. Chem. Phys.*, **11**, 2111–2125, https://doi.org/10.5194/acp-11-2111-2011.

——, C. H. Halios, S. E. Lane, and C. R. Wood, 2015: Observations of urban boundary layer structure during a strong urban heat island event. *Environ. Fluid Mech.*, **15**, 373–398, https://doi.org/10.1007/s10652-014-9335-6.

Blackadar, A. K., 1957: Boundary Layer Wind Maxima and Their Significance for the Growth of Nocturnal Inversions. *Bull. Am. Meteorol. Soc.*, **38**, 283–290, https://doi.org/10.1175/1520-0477-38.5.283.

Bonner, W. D., 1968: Climatology of the Low Level Jet. *Mon. Weather Rev.*, **96**, 833–850,

https://doi.org/10.1175/1520-0493(1968)096<0833:cotllj>2.0.co;2.

Bornstein, R., 1968: Observations of the Urban Heat Island Effect in New York City. *J. Appl. Meteorol.*, **7**, 575–582, https://doi.org/https://doi.org/10.1175/1520-0450(1968)007<0575:OOTUHI>2.0.CO;2.

Brunekreef, B., and S. T. Holgate, 2002: Air pollution and health. *Lancet*, **360**, 1233–1242, https://doi.org/10.1016/S0140-6736(02)11274-8.

Cosgrove, A., and M. Berkelhammer, 2018: Downwind footprint of an urban heat island on air and lake temperatures. *npj Clim. Atmos. Sci.*, **1**, 1–10, https://doi.org/10.1038/s41612-018-0055-3.

Dai, C., Q. Wang, J. A. Kalogiros, D. H. Lenschow, Z. Gao, and M. Zhou, 2014: Determining Boundary-Layer Height from Aircraft Measurements. *Boundary-Layer Meteorol.*, **152**, 277–302, https://doi.org/10.1007/s10546-014-9929-z.

Drüe, C., T. Hauf, and A. Hoff, 2010: Comparison of boundary-layer profiles and layer detection by AMDAR and WTR/RASS at Frankfurt airport. *Boundary-Layer Meteorol.*, **135**, 407–432, https://doi.org/10.1007/s10546-010-9485-0.

Garratt, J. R., 1990: The internal boundary layer - A review. *Boundary-Layer Meteorol.*, **50**, 171–203, https://doi.org/10.1007/BF00120524.

Global Energy Assessment Writing Team, 2012: *Global Energy Assessment*. Cambridge University Press,.

Grimmond, C. S. B., 2006: Progress in measuring and observing the urban atmosphere. *Theor. Appl. Climatol.*, **84**, 3–22, https://doi.org/10.1007/s00704-005-0140-5.

Guttman, N. B., and C. B. Baker, 1996: Exploratory analysis of the difference between temperature observations recorded by ASOS and conventional methods. *Bull. Am.*

Meteorol. Soc., **77**, 2865–2873, https://doi.org/10.1175/1520-0477(1996)077<2865:EAOTDB>2.0.CO;2.

Halios, C. H., and J. F. Barlow, 2018: Observations of the Morning Development of the Urban Boundary Layer Over London, UK, Taken During the ACTUAL Project. *Boundary-Layer Meteorol.*, **166**, 395–422, https://doi.org/10.1007/s10546-017-0300-z.

Haman, C. L., B. Lefer, and G. A. Morris, 2012: Seasonal Variability in the Dirunal Evolution of the Boundary Layer in a Near-Coastal Urban Environment. *J. Atmos. Ocean. Technol.*, **29**, 697–710, https://doi.org/10.1175/JTECH-D-11-00114.1.

Hanna, S. R., 1969: The thickness of the planetary boundary layer. *Atmos. Environ.*, **3**, 519–536, https://doi.org/10.1016/0004-6981(69)90042-0.

Hennemuth, B., and A. Lammert, 2006: Determination of the atmospheric boundary layer height from radiosonde and lidar backscatter. *Boundary-Layer Meteorol.*, **120**, 181–200, https://doi.org/10.1007/s10546-005-9035-3.

Holton, J. R., 1967: The diurnal boundary layer wind oscillation above sloping terrain. *Tellus*, **19**, 200–205, https://doi.org/10.3402/tellusa.v19i2.9766.

Hu, X. M., P. M. Klein, M. Xue, J. K. Lundquist, F. Zhang, and Y. Qi, 2013: Impact of low-level jets on the nocturnal urban heat island intensity in Oklahoma city. *J. Appl. Meteorol. Climatol.*, **52**, 1779–1802, https://doi.org/10.1175/JAMC-D-12-0256.1.

Kallistratova, M. A., and R. D. Kouznetsov, 2012: Low-Level Jets in the Moscow Region in Summer and Winter Observed with a Sodar Network. *Boundary-Layer Meteorol.*, **143**, 159–175, https://doi.org/10.1007/s10546-011-9639-8.

Klein, P. M., X. M. Hu, A. Shapiro, and M. Xue, 2016: Linkages Between Boundary-Layer Structure and the Development of Nocturnal Low-Level Jets in Central Oklahoma.

Boundary-Layer Meteorol., **158**, 383–408, https://doi.org/10.1007/s10546-015-0097-6.

Kotthaus, S., and C. S. B. Grimmond, 2018a: Atmospheric boundary-layer characteristics from ceilometer measurements. Part 1: A new method to track mixed layer height and classify clouds. *Q. J. R. Meteorol. Soc.*, **144**, 1525–1538, https://doi.org/10.1002/qj.3299.

——, and ——, 2018b: Atmospheric boundary-layer characteristics from ceilometer measurements. Part 2: Application to London's urban boundary layer. *Q. J. R. Meteorol. Soc.*, **144**, 1511–1524, https://doi.org/10.1002/qj.3298.

Lapworth, A., 2006: The morning transition of the nocturnal boundary layer. *Boundary-Layer Meteorol.*, **119**, 501–526, https://doi.org/10.1007/s10546-005-9046-0.

Li, Z., and Coauthors, 2017: Aerosol and boundary-layer interactions and impact on air quality. *Natl. Sci. Rev.*, **4**, 810–833, https://doi.org/10.1093/nsr/nwx117.

Lund, R., X. L. Wang, Q. Q. Lu, J. Reeves, C. Gallagher, and Y. Feng, 2007: Changepoint detection in periodic and autocorrelated time series. *J. Clim.*, **20**, 5178–5190, https://doi.org/10.1175/JCLI4291.1.

Macdonald, R. W., 2000: Modelling the mean velocity profile in the urban canopy layer. *Boundary-Layer Meteorol.*, **97**, 25–45, https://doi.org/10.1023/A:1002785830512.

Magee, N., J. Curtis, and G. Wendler, 1999: The Urban Heat Island Effect at Fairbanks, Alaska. *Theor. Appl. Climatol.*, **64**, 39–47, https://doi.org/10.1007/s007040050109.

Mahrt, L., 2000: Surface heterogeneity and vertical structure of the boundary layer. *Boundary-Layer Meteorol.*, **96**, 33–62, https://doi.org/10.1023/A:1002482332477.

Nowak, D. J., and J. T. Walton, 2005: Projected Urban Growth (2000–2050) and Its Estimated Impact on the US Forest Resource. *J. For.*, **103**, 383–389, https://doi.org/10.1093/jof/103.8.383.

Nowak, D. J., and E. J. Greenfield, 2018: US urban forest statistics, values, and projections. *J. For.*, **116**, 164–177, https://doi.org/10.1093/jofore/fvx004.

Nunez, M., and T. R. Oke, 1977: The Energy Balance of an Urban Canyon. *J. Appl. Meteorol.*, **16**, 11–19, https://doi.org/10.1175/1520-0450(1977)016<0011:TEBOAU>2.0.CO;2.

Oke, T. R., 1987: *Boundary Layer Climates*. 2nd ed. Routledge: Taylor & Francis Group, 288–294 pp.

Pal, S., and M. Haeffelin, 2015: Forcing mechanisms governing diurnal, seasonal, and interannual variability in the boundary layer depths: Five years of continuous lidar observations over a suburban site near Paris. *J. Geophys. Res. Atmos.*, **120**, 238–238, https://doi.org/10.1002/2015JD023268.

Petäjä, T., and Coauthors, 2016: Enhanced air pollution via aerosol-boundary layer feedback in China. *Sci. Rep.*, **6**, 1–6, https://doi.org/10.1038/srep18998.

Reeves, J., J. Chen, X. L. Wang, R. Lund, and Q. Q. Lu, 2007: A review and comparison of changepoint detection techniques for climate data. *J. Appl. Meteorol. Climatol.*, **46**, 900–915, https://doi.org/10.1175/JAM2493.1.

Rotach, M. W., 1999: On the influence of the urban roughness sublayer on turbulence and dispersion. *Atmos. Environ.*, **33**, 4001–4008, https://doi.org/10.1016/S1352-2310(99)00141-7.

Ryu, Y. H., and J. J. Baik, 2012: Quantitative analysis of factors contributing to urban heat island intensity. *J. Appl. Meteorol. Climatol.*, **51**, 842–854, https://doi.org/10.1175/JAMC-D-11-098.1.

Sailor, D. J., 2011: A review of methods for estimating anthropogenic heat and moisture emissions in the urban environment. *Int. J. Climatol.*, **31**, 189–199,

https://doi.org/10.1002/joc.2106.

Salamanca, F., A. Krpo, A. Martilli, and A. Clappier, 2009: A new building energy model coupled with an urban canopy parameterization for urban climate simulations—part I. formulation, verification, and sensitivity analysis of the model. *Theor. Appl. Climatol.*, **99**, 331, https://doi.org/10.1007/s00704-009-0142-9.

Sarnat, J. A., J. Schwartz, P. J. Catalano, and H. H. Suh, 2001: Gaseous pollutants in particulate matter epidemiology: Confounders or surrogates? *Environ. Health Perspect.*, **109**, 1053–1061, https://doi.org/10.1289/ehp.011091053.

Schrijvers, P. J. C., H. J. J. Jonker, S. Kenjereš, and S. R. de Roode, 2015: Breakdown of the night time urban heat island energy budget. *Build. Environ.*, **83**, 50–64, https://doi.org/10.1016/j.buildenv.2014.08.012.

Seidel, D. J., Y. Zhang, A. Beljaars, J. C. Golaz, A. R. Jacobson, and B. Medeiros, 2012: Climatology of the planetary boundary layer over the continental United States and Europe. *J. Geophys. Res. Atmos.*, **117**, 1–15, https://doi.org/10.1029/2012JD018143.

Seto, K., M. Fragkias, B. Guneralp, and M. Reilly, 2011: A meta-analysis of global urban land expansion. *PLoS One*, **6**, https://doi.org/10.1371/journal.pone.0023777.

Shepherd, J. M., 2005: A review of current investigations of urban-induced rainfall and recommendations for the future. *Earth Interact.*, **9**, https://doi.org/10.1175/EI156.1.

Steeneveld, G. J., S. Koopmans, B. G. Heusinkveld, L. W. A. Van Hove, and A. A. M. Holtslag, 2011: Quantifying urban heat island effects and human comfort for cities of variable size and urban morphology in the Netherlands. *J. Geophys. Res. Atmos.*, **116**, 1–14, https://doi.org/10.1029/2011JD015988.

Stoll, R., J. A. Gibbs, S. T. Salesky, W. Anderson, and M. Calaf, 2020: Large-Eddy Simulation

of the Atmospheric Boundary Layer. *Boundary-Layer Meteorol.*, **177**, 541–581, https://doi.org/10.1007/s10546-020-00556-3.

Tolias, I. C., N. Koutsourakis, D. Hertwig, G. C. Efthimiou, A. G. Venetsanos, and J. G. Bartzis, 2018: Large Eddy Simulation study on the structure of turbulent flow in a complex city. *J. Wind Eng. Ind. Aerodyn.*, **177**, 101–116, https://doi.org/10.1016/j.jweia.2018.03.017.

United Nations, 2011: *World Urbanization Prospects: The 2011 Revision*.

Vogelezang, D. H. P., and A. A. M. Holtslag, 1996: Evaluation and model impacts of alternative boundary-layer height formulations. *Boundary-Layer Meteorol.*, **81**, 245–269, https://doi.org/10.1007/BF02430331.

Wagner, T. J., and J. M. Kleiss, 2016: Error characteristics of ceilometer-based observations of cloud amount. *J. Atmos. Ocean. Technol.*, **33**, 1557–1567, https://doi.org/10.1175/JTECH-D-15-0258.1.

Wang, Y., C. L. Klipp, D. M. Garvey, D. A. Ligon, C. C. Williamson, S. S. Chang, R. K. Newsom, and R. Calhoun, 2007: Nocturnal low-leveL-jet-dominated atmospheric boundary layer observed by a Doppler lidar over Oklahoma City during JU2003. *J. Appl. Meteorol. Climatol.*, **46**, 2098–2109, https://doi.org/10.1175/2006JAMC1283.1.

——, J. Decker, and E. R. Pardyjak, 2020: Large-eddy simulations of turbulent flows around buildings using the Atmospheric Boundary Layer Environment-Lattice Boltzmann Model (ABLE-LBM). *J. Appl. Meteorol. Climatol.*, **59**, 885–899, https://doi.org/10.1175/JAMC-D-19-0161.1.

Whiteman, C. D., X. Bian, and S. Zhong, 1997: Low-level jet climatology from enhanced rawinsonde observations at a site in the southern Great Plains. *J. Appl. Meteorol.*, **36**, 1363–1376, https://doi.org/10.1175/1520-0450(1997)036<1363:LLJCFE>2.0.CO;2.

Wood, N., and P. Mason, 1991: The influence of static stability on the effective roughness lengths for momentum and heat transfer. *Q. J. R. Meteorol. Soc.*, **117**, 1025–1056, https://doi.org/10.1002/qj.49711750108.

World Meteorological Organization, 2014: *The Benefits of AMDAR Data to Meteorology and Aviation*.

——, 2015: *Impact and Benefits of AMDAR Temperature, Wind and Moisture Observations in Operational Weather Forecasting*.

——, 2017: *Guide to Aircraft-based Observations*.

——, 2018: *WIGOS, WMO Integrated Global Observing System - Benefits to the Environment and Society from the Availability and Use of AMDAR Data*.

Yuval, Y. Levi, U. Dayan, I. Levy, and D. M. Broday, 2020: On the association between characteristics of the atmospheric boundary layer and air pollution concentrations. *Atmos. Res.*, **231**, 104675, https://doi.org/10.1016/j.atmosres.2019.104675.

Zhang, Y., Z. Gao, D. Li, Y. Li, N. Zhang, X. Zhao, and J. Chen, 2014: On the computation of planetary boundary-layer height using the bulk Richardson number method. *Geosci. Model Dev.*, **7**, 2599–2611, https://doi.org/10.5194/gmd-7-2599-2014.

Zhang, Y., D. Li, Z. Lin, J. A. Santanello, and Z. Gao, 2019: Development and Evaluation of a Long-Term Data Record of Planetary Boundary Layer Profiles From Aircraft Meteorological Reports. *J. Geophys. Res. Atmos.*, **124**, 2008–2030, https://doi.org/10.1029/2018JD029529.

——, K. Sun, Z. Gao, Z. Pan, M. A. Shook, and D. Li, 2020: Diurnal Climatology of Planetary Boundary Layer Height Over the Contiguous United States Derived From AMDAR and Reanalysis Data. *J. Geophys. Res. Atmos.*, **125**, 1–21,

https://doi.org/10.1029/2020JD032803.

Appendix

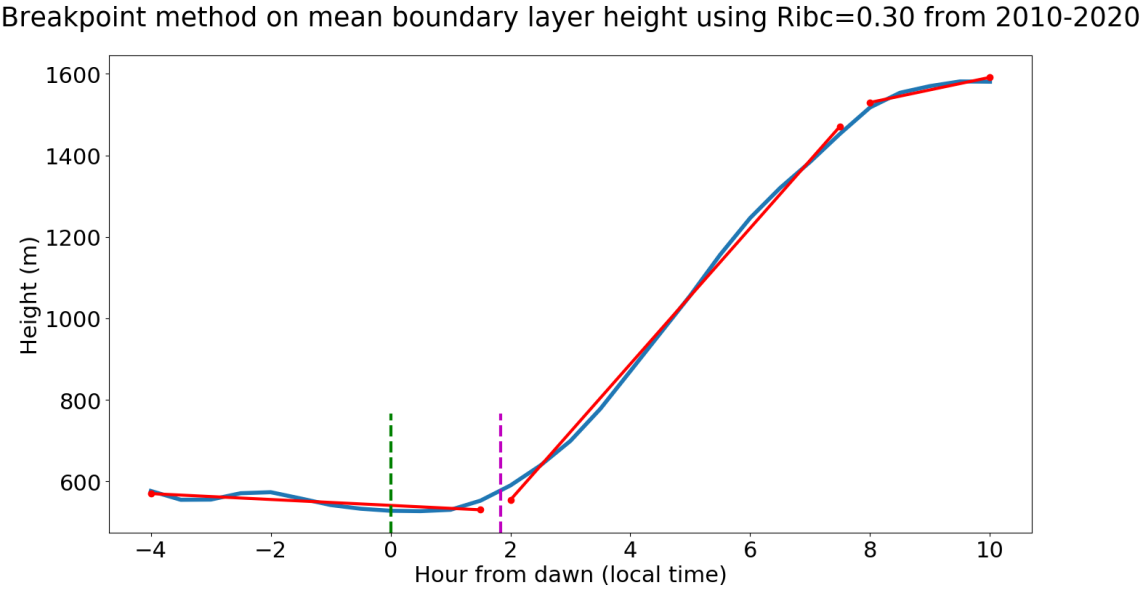

Figure A.1. Breakpoint method using the mean mixed layer height with a Ri_{bc} of 0.30. The green dashed vertical line represents dawn, and the purple dashed vertical line represents the end of the morning transition, giving a total duration of 1.839 hours.

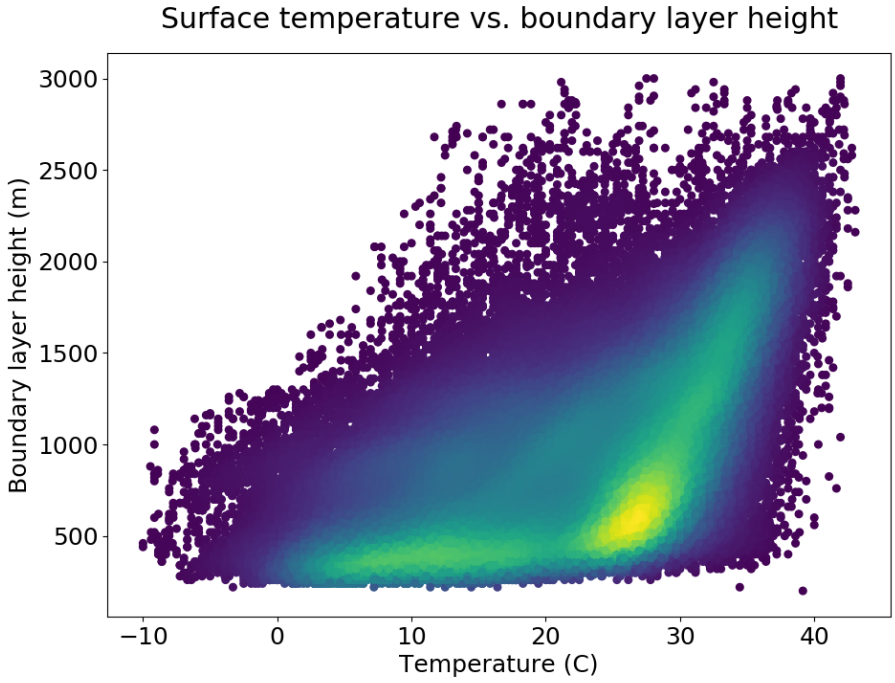

Figure A.2. Surface temperature compared with BL height.

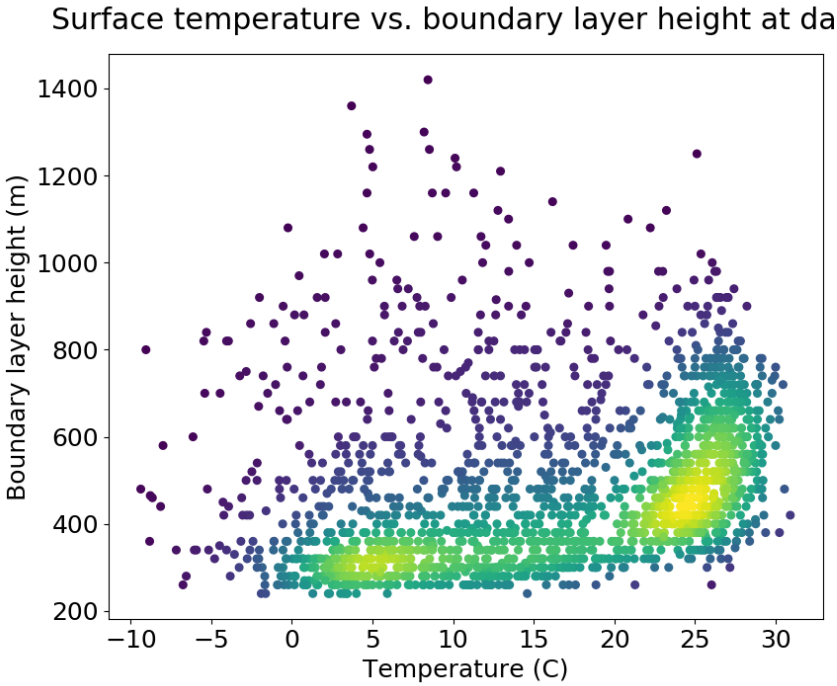

Figure A.3. Same as Figure A.2 but at dawn.